Next Generation Benchmark Control Problem for Seismically Excited Buildings

B.F. Spencer Jr.,[1] R.E. Christenson[2] and S.J. Dyke[3]

Abstract

This paper presents the problem definition and guidelines of the next generation structural control benchmark problem for seismically excited buildings. Focusing on a 20-story steel structure representing a typical mid- to high-rise building designed for the Los Angeles, California region, the goal of this study is to provide a clear basis to evaluate the efficacy of various structural control strategies. An *evaluation* model has been developed that portrays the salient features of the structural system. Control constraints and evaluation criteria are presented for the design problem. The task of each participant in this benchmark study is to define (including devices, sensors and control algorithms), evaluate and report on their proposed control strategies. These strategies may be either passive, active, semi-active or a combination thereof. A simulation program has been developed and made available to facilitate direct comparison of the efficiency and merit of the various control strategies. To illustrate some of the design challenges a sample control system design is presented, although this sample is not intended to be viewed as a competitive design.

Introduction

The protection of civil structures, including material content and human occupants, is without a doubt a world-wide priority. The extent of protection may range from reliable operation and occupant comfort to human and structural survivability. Civil structures, including existing and future buildings, towers and bridges, must be adequately protected from a variety of events, including earthquakes, winds, waves and traffic. The protection of structures is now moving from relying entirely on the inelastic deformation of the structure to dissipate the energy of severe dynamic loadings, to the application of passive, active and semi-active structural control devices to mitigate undesired responses to dynamic loads.

In the last two decades, many control algorithms and devices have been proposed for civil engineering applications (Soong 1990; Housner, *et al*. 1994; Soong and Constantinou 1994; Fujino, *et al*. 1996; Spencer and Sain 1997), each of which has certain advantages, depending on the specific application and the desired objectives. At the present time, structural control research is greatly diversified with regard to these specific applications and desired objectives. A common basis for comparison of the various algorithms and devices does not currently exist. Determina-

1. Prof., Dept. of Civil Engrg. and Geo. Sci., Univ. of Notre Dame, Notre Dame, IN 46556-0767.
2. Doc. Cand., Dept. of Civil Engrg. and Geo. Sci., Univ. of Notre Dame, Notre Dame, IN 46556-0767.
3. Assist. Prof., Dept. of Civil Engrg., Washington Univ., St. Louis, MO 63130-4899.

tion of the general effectiveness of structural control algorithms and devices, a task which is necessary to focus future structural control research and development, is challenging.

Ideally, each proposed control strategy should be evaluated experimentally under conditions that closely model the as-built environment. However, it is impractical, both financially and logistically, for all researchers in structural control to conduct even small-scale experimental tests. An available alternative is the use of consensus-approved, high-fidelity, analytical benchmark models to allow researchers in structural control to test their algorithms and devices and to directly compare the results.

The American Society of Civil Engineers (ASCE) Committee on Structural Control has recognized the significance of structural control benchmark problems. The Committee recently developed a benchmark study, focusing primarily on the comparison of structural control algorithms for three-story building models. The initial results of this study were reported at the 1997 ASCE Structures Congress, held in Portland, Oregon (Spencer, *et al*. 1997; Balas, 1997; Lu and Skelton 1997; Wu, *et al*. 1997; Smith, *et al*. 1997). Additionally, a more extensive analysis of the benchmark structural control problem is nearing completion and will form the basis for a special issue of *Earthquake Engineering and Structural Dynamics* (Spencer, *et al*. 1998).

Building on the foundation laid by the ASCE Committee on Structural Control, plans for the next generation of benchmark structural control studies were initiated by the Working Group on Building Control during the Second International Workshop on Structural Control held December 18–20, 1996, in Hong Kong (Chen 1996). As stated by the Working Group, the goal of this effort is to develop benchmark models to provide systematic and standardized means by which competing control strategies, including devices, algorithms, sensors, *etc*., can be evaluated. This goal drives the next generation of structural control benchmark problems, and its achievement will take the structural control community another step toward the realization and implementation of innovative control strategies for dynamic hazard mitigation.

As an outgrowth of the workshop in Hong Kong, two benchmark problems for the control of buildings have been developed for presentation at the 2nd World Conference on Structural Control to be held June 28–July 1, 1998 in Kyoto, Japan. The first, detailed in Yang, *et al*. (1998), proposes a benchmark problem for wind excited buildings. The second such benchmark problem is defined herein, the focus of which is to provide the guidelines for the next generation benchmark control problem for seismically excited buildings. A 20-story steel building designed for the SAC[4] project is the benchmark structure to be studied. A description of this structure is discussed in the next section. A high-fidelity linear time-invariant state space model of this structure was developed and is designated the *evaluation* model. In the context of this study, the evaluation model is considered to be a true model of the structural system. Several evaluation criteria, measuring the effectiveness of the control strategy to reduce undesired responses of the evaluation model to ground excitation, are given, along with the associated control design constraints.

4. SAC is a joint venture of three non-profit organizations: The Structural Engineers Association of California (SEAOC), the Applied Technology Council (ATC) and California Universities for Research in Earthquake Engineering (CUREE). SAC Steel Project Technical Office, 1301 S. 46th Street, Richmond, CA 94804-4698. http://quiver.eerc.berkeley.edu:8080/.

Designers/researchers participating in this benchmark study shall define (including devices, sensors and control algorithms), evaluate and report the results for their proposed control strategies. The location on the structure and an appropriate model must be specified for each control device and sensor employed. Passive, active and semi-active devices, or a combination thereof, may be considered. For illustrative purposes a complete sample control design is presented. Although this sample control system it not intended to be competitive, it demonstrates how one might define and model the sensors and control devices employed, build a design model, and evaluate a complete control system design.

Benchmark Structure

The 20-story structure used for this benchmark study was designed by Brandow & Johnston Associates[5] for the SAC Phase II Steel Project. Although not actually constructed, the structure meets seismic code and represents a typical mid- to high-rise building designed for the Los Angeles, California region. This building was chosen because it will also serve as a benchmark structure for SAC studies and thus will provide a wider basis for comparison of the results from the present study.

The Los Angeles twenty-story (LA 20-story) structure is 30.48 m (100 ft) by 36.58 m (120 ft) in plan, and 80.77 m (265 ft) in elevation. The bays are 6.10 m (20 ft) on center, in both directions, with five bays in the north-south (N-S) direction and six bays in the east-west (E-W) direction. The building's lateral load-resisting system is comprised of steel perimeter moment-resisting frames (MRFs). The interior bays of the structure contain simple framing with composite floors.

The columns are 345 Mpa (50 ksi) steel. The interior columns of the MRF are wide-flange. The corner columns are box columns. The levels of the 20-story building are numbered with respect to the first story, located at the ground (first) level (see Fig. 1). The 21st level is denoted the roof. The building has an additional two basement levels. The level directly below the ground level is the second basement (B-2). The level below B-2 is the first basement (B-1). Typical floor-to-floor heights (for analysis purposes measured from center-of-beam to center-of-beam) are 3.96 m (13 ft). The floor-to-floor heights for the two basement levels are 3.65 m (12 ft) and for the first floor is 5.49 m (18 ft).

The column lines employ three-tier construction, *i.e.* monolithic column pieces are connected every three levels beginning with the second story. Column splices, which are seismic (tension) splices to carry bending and uplift forces, are located on the 2nd, 5th, 8th, 11th, 14th, 17th and 19th stories at 1.83 m (6 ft) above the center-line of the beam to column joint. The column bases are modeled as pinned (at the B-1 level) and secured to the ground. Concrete foundation walls and surrounding soil are assumed to restrain the structure at the first floor from horizontal displacement.

The floors are composite construction (*i.e.*, concrete and steel). In accordance with common practice, the floor system, which provides diaphragm action, is assumed to be rigid in the horizon-

5. Brandow & Johnston Associates, Consulting Structural Engineers, 1660 W. Third St., Los Angeles, CA 90017.

tal plane. The floor system is comprised of 248 Mpa (36 ksi) steel wide-flange beams acting compositely with the floor slab. The B-2 floor beams are simply connected to the columns. The inertial effects of each level are assumed to be carried evenly by the floor diaphragm to each perimeter MRF, hence each frame resists one half of the seismic mass associated with the entire structure.

The seismic mass of the structure is due to various components of the structure, including the steel framing, floor slabs, ceiling/flooring, mechanical/electrical, partitions, roofing and a penthouse located on the roof. The seismic mass of the first level is 5.32×10^5 kg (36.4 kips-sec^2/ft), for the second level is 5.65×10^5 kg (38.7 kips-sec^2/ft), for the third level to 20th level is 5.51×10^5 kg (37.7 kips-sec^2/ft), and for the roof is 5.83×10^5 kg (39.9 kips-sec^2/ft). The seismic mass of the entire structure is 1.16×10^7 kg (794 kips-sec^2/ft).

This benchmark study will focus on an in-plane (2-D) analysis of one-half of the entire structure. The frame being considered in this study is one of the N-S MRFs (the short direction of the building). The height to width ratio for the N-S frame is 2.65:1. The N-S MRF is depicted in Fig. 1.

Passive, active and/or semi-active control devices can be implemented throughout the N-S frame of the 20-story structure and their performance assessed using the evaluation models specified in the next section.

Evaluation Model

Based on the physical description of the LA 20-story structure described in the previous section, an in-plane finite element model of the N-S MRF is developed in MATLAB (1997). Because the focus of this study is on global response characteristics, considering the linearized response of the structure can be shown to be a reasonable approximation (Naeim 1997) that will be used for the purposes of this study. The structure is modeled as a system of plane-frame elements, and mass and stiffness matrices for the structure are determined. Due to the size of the model, a Guyan reduction is used to reduce the number of DOFs to a manageable size, while still maintaining the important dynamics of the full model. Using the reduced mass and stiffness matrices, the damping matrix is determined based on an assumption of modal damping. The equations of motion for the structure are then developed in a state space form appropriate for design and analysis. This process, described in further detail in the following paragraphs, is illustrated in Fig. 2.

The LA 20-story structure is modeled using 180 nodes interconnected by 284 elements, as seen in Fig. 3. The nodes are located at beam-to-column joints and at column splice locations. Elements are created between nodes to represent the beams and columns in the structure. The beam members extend from the center-line of column to center-line of column, thus ignoring the column panel zone. Floor inertial loads, accounting for the seismic mass of the floor slabs, ceiling/flooring, mechanical/electrical, partitions, roofing and penthouse are uniformly distributed at the nodes of each respective floor assuming a consistent mass formulation.

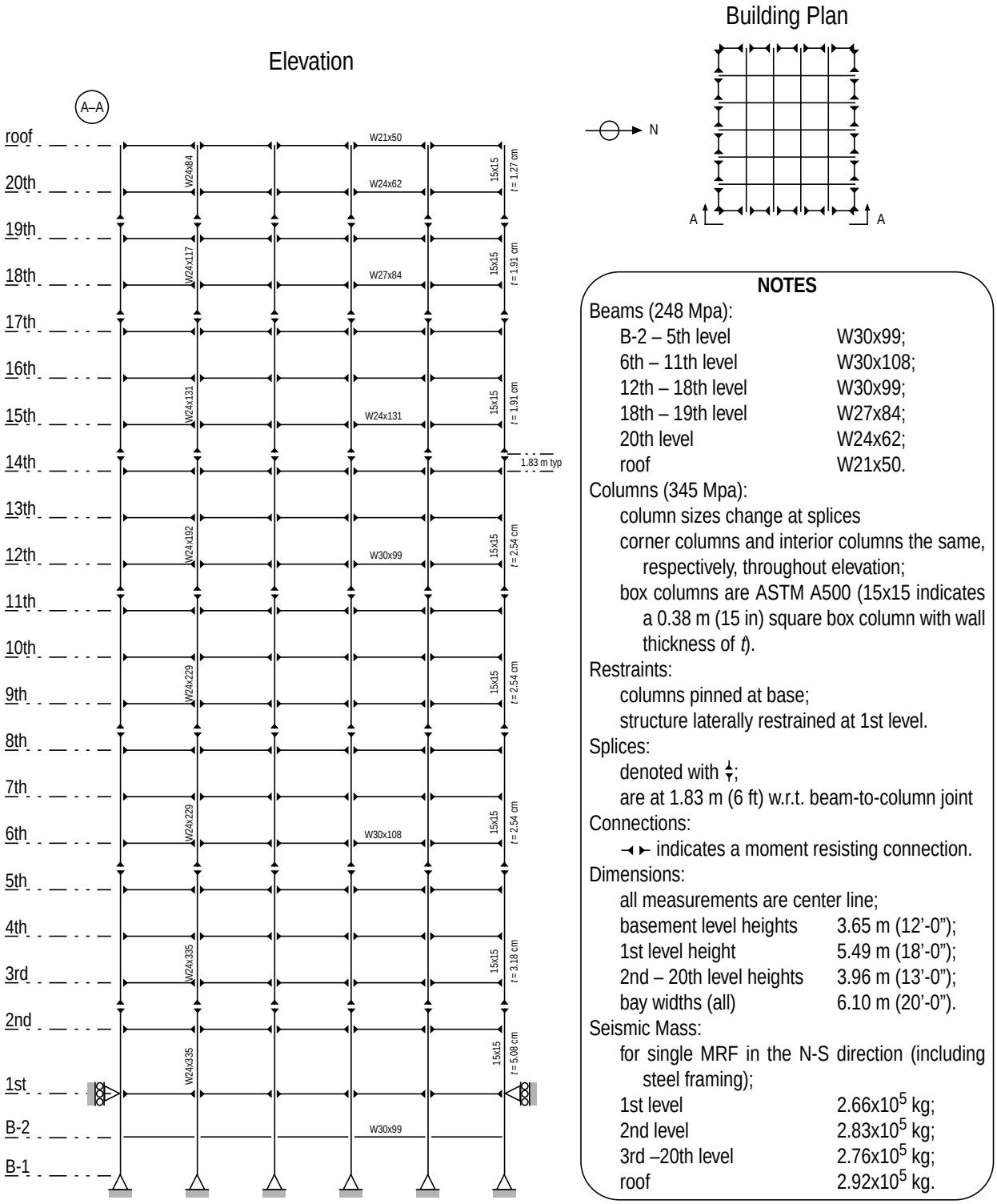

NOTES

Beams (248 Mpa):

B-2 – 5th level	W30x99;
6th – 11th level	W30x108;
12th – 18th level	W30x99;
18th – 19th level	W27x84;
20th level	W24x62;
roof	W21x50.

Columns (345 Mpa):

- column sizes change at splices
- corner columns and interior columns the same, respectively, throughout elevation;
- box columns are ASTM A500 (15x15 indicates a 0.38 m (15 in) square box column with wall thickness of *t*).

Restraints:

- columns pinned at base;
- structure laterally restrained at 1st level.

Splices:

- denoted with ⇕;
- are at 1.83 m (6 ft) w.r.t. beam-to-column joint

Connections:

- ⊣ ⊢ indicates a moment resisting connection.

Dimensions:

- all measurements are center line;

basement level heights	3.65 m (12'-0");
1st level height	5.49 m (18'-0");
2nd – 20th level heights	3.96 m (13'-0");
bay widths (all)	6.10 m (20'-0").

Seismic Mass:

- for single MRF in the N-S direction (including steel framing);

1st level	2.66×10^5 kg;
2nd level	2.83×10^5 kg;
3rd –20th level	2.76×10^5 kg;
roof	2.92×10^5 kg.

Figure 1: Los Angeles 20-Story Building N-S MRF.

Each node has three degrees-of-freedom (DOFs): horizontal, vertical and rotational. The entire structure has 540 DOFs prior to application of boundary conditions/constraints and subsequent model reduction. Global DOF n is the jth local DOF (*i.e.*, horizontal: $j = 1$, vertical: $j = 2$, rotation: $j = 3$) of the ith node as given by $n = 3(i-1) + j$.

The evaluation model focuses on one of the two N-S MRFs of the LA-20 story structure. This single N-S frame is assumed to support one half of the seismic mass of the entire structure (*i.e.*, 2.66×10^5 kg (18.2 kips-sec^2/ft) for the first level, 2.83×10^5 kg (19.4 kips-sec^2/ft) for the second level, 2.76×10^5 kg (18.9 kips-sec^2/ft) for the third to 20th levels, and 2.92×10^5 kg (20.0 kips-sec^2/ft) for the roof). Additionally, for modeling purposes, the seismic mass is broken into two components: the steel framing, including beams and columns, and all other additional seismic mass. The seismic mass of the steel framing of a single N-S MRF is 2.64×10^5 kg (18.1 kips-sec^2/ft). The seismic mass of a single N-S MRF, without the mass of the steel framing, for the first level is 2.54×10^5 kg (17.4 kips-sec^2/ft), for the second level is 2.70×10^5 kg (18.5 kips-sec^2/ft), for the third level to 20th level is 2.63×10^5 kg (18.0 kips-sec^2/ft) and for the roof is 2.79×10^5 kg (19.1 kips-sec^2/ft). The seismic mass of the N-S MRF is 5.80×10^6 kg (397 kips-sec^2/ft). The seismic mass of all above ground floors of the N-S MRF, neglecting the mass of the first level, is 5.543×10^6 kg (379 kips-sec^2/ft).

Each element, modeled as a plane frame element, contains two nodes and six DOFs. The length, area, moment of inertia, modulus of elasticity and mass density are pre-defined for each element. The elemental consistent mass and stiffness matrices are determined as functions of these properties (Sack 1989; Cook, *et. al* 1989).

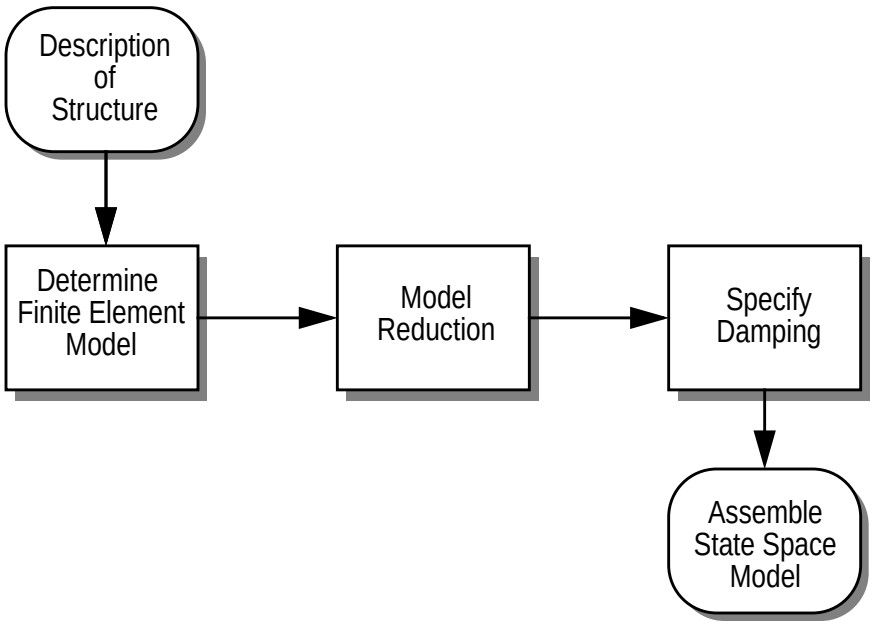

Figure 2: Schematic of Finite Element Model to Form the Evaluation Model for Los Angeles 20-Story Structure.

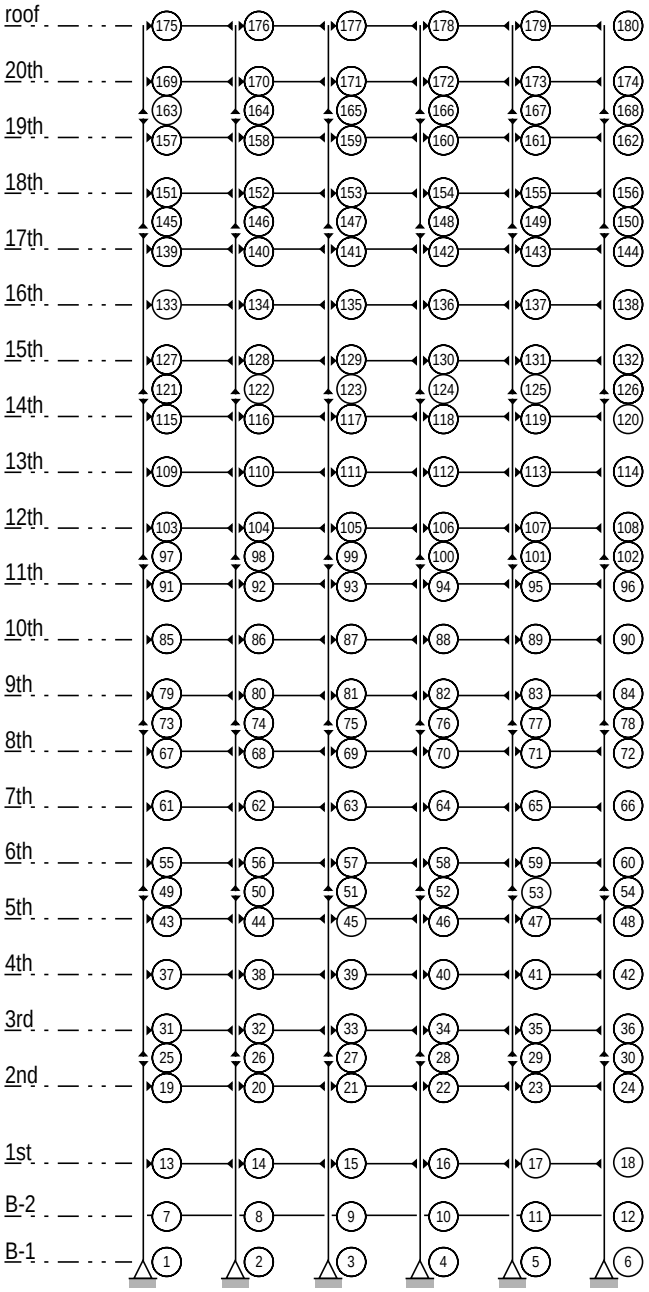

Figure 3: Node Numbers for the Los Angeles 20-Story Structure's N-S MRF.

Global mass and stiffness matrices are assembled from the elemental mass and stiffness matrices by summing the mass and stiffness associated with each DOF for each element of the entire structure. The DOFs corresponding to fixed boundary conditions are then constrained by eliminating the rows and columns associated with these DOFs from the global mass and stiffness matrices. The constrained DOFs are the horizontal DOFs at nodes 1, 2, 3, 4, 5, 6, 13 and 18 and the vertical DOFs at nodes 1, 2, 3, 4, 5 and 6. Realizing these 14 boundary conditions results in

the mass matrix, $\mathbf{M}$ [526×526], and the stiffness matrix, $\mathbf{K}$ [526×526]. The equation of motion for the undamped structural system takes the form

$$\mathbf{M}\ddot{\mathbf{U}} + \mathbf{K}\mathbf{U} = -\mathbf{M}\boldsymbol{\Gamma}\ddot{x}_g + \mathbf{P}\mathbf{f} \tag{1}$$

where $\ddot{\mathbf{U}}$ is the second time derivative of the response vector $\mathbf{U}$, $\ddot{x}_g$ (m/sec^2) is the ground acceleration, $\mathbf{f}$ (kN) is the control force input, $\boldsymbol{\Gamma}$ is a vector of zeros and ones defining the loading of the ground acceleration to the structure, and $\mathbf{P}$ is a vector defining how the force(s) produced by the control device(s) enter the structure. Responses for a particular level are measured at the floor of the level in question. The horizontal responses are relative to the ground.

Because the floor slab is assumed to be rigid in its horizontal plane, the nodes associated with each floor have the same horizontal displacements. This assumption is enforced by writing constraint equations relating the dependent (slave) horizontal DOFs on each floor slab to a single active horizontal DOF and using a Ritz transformation (Craig, 1981). First, the structural responses are partitioned in terms of active and dependent DOFs as $\mathbf{U} = [\mathbf{U}_a^T \ \mathbf{U}_d^T]^T$, and the constraint equations are written in the form $\mathbf{R}_{da}\mathbf{U}_a + \mathbf{R}_{dd}\mathbf{U}_d = \mathbf{0}$. The mass and stiffness matrices are similarly partitioned in terms of active and dependent DOFs

$$\mathbf{M} = \begin{bmatrix} \mathbf{M}_{aa} & \mathbf{M}_{ad} \\ \mathbf{M}_{da} & \mathbf{M}_{dd} \end{bmatrix}, \qquad \mathbf{K} = \begin{bmatrix} \mathbf{K}_{aa} & \mathbf{K}_{ad} \\ \mathbf{K}_{da} & \mathbf{K}_{dd} \end{bmatrix} \tag{2}$$

Reducing out the dependent DOFs yields

$$\hat{\mathbf{M}}\ddot{\mathbf{U}}_a + \hat{\mathbf{K}}\mathbf{U}_a = -\hat{\mathbf{G}}\ddot{x}_g + \hat{\mathbf{P}}\mathbf{f} \tag{3}$$

where

$$\begin{aligned} \hat{\mathbf{M}} &= \mathbf{T}_R^T\mathbf{M}\mathbf{T}_R, \qquad \hat{\mathbf{K}} = \mathbf{T}_R^T\mathbf{K}\mathbf{T}_R \\ \hat{\mathbf{G}} &= \mathbf{T}_R^T\mathbf{M}\boldsymbol{\Gamma}, \qquad \hat{\mathbf{P}} = \mathbf{T}_R^T\mathbf{P} \end{aligned} \tag{4}$$

and

$$\mathbf{T}_R = \begin{bmatrix} \mathbf{I} \\ \mathbf{T}_{da} \end{bmatrix}, \qquad \mathbf{T}_{da} = -\mathbf{R}_{dd}^{-1}\mathbf{R}_{da} \tag{5}$$

$\mathbf{I}$ is an appropriately sized identity matrix. Note that $\boldsymbol{\Gamma}$ and $\mathbf{P}$ also must be reordered corresponding to the active and dependent DOFs prior to making the transformation in Eq. (4). The number of DOFs in the resulting model is 418.

The next step in forming the evaluation model is model reduction. A model with 418 DOFs is computationally burdensome for dynamic analysis. The natural frequencies of the higher modes

in this model are excessively large. As these modes, attributed mostly to rotational and vertical DOFs, are unlikely to contribute to the response of the physical system, they are not required for the benchmark model and can be reduced out. A Guyan reduction (Craig 1981) of all of the rotational and most of the vertical DOFs is used to reduce the 418 DOF model to nearly 1/5 of its original size.

Again, the DOFs are partitioned into active and dependent (slave) DOFs. The active horizontal DOFs, as well as the vertical DOFs for levels 1–21 located on the second and fifth column lines, are chosen to be active. All other vertical DOFs, including the vertical DOFs at splice locations, and all rotational DOFs are assumed dependent and condensed out. The mass and stiffness matrices are partitioned in terms of the active and dependent degrees of freedom, *i.e.*,

$$\hat{\mathbf{M}} = \begin{bmatrix} \hat{\mathbf{M}}_{aa} & \hat{\mathbf{M}}_{ad} \\ \hat{\mathbf{M}}_{da} & \hat{\mathbf{M}}_{dd} \end{bmatrix}, \qquad \hat{\mathbf{K}} = \begin{bmatrix} \hat{\mathbf{K}}_{aa} & \hat{\mathbf{K}}_{ad} \\ \hat{\mathbf{K}}_{da} & \hat{\mathbf{K}}_{dd} \end{bmatrix} \tag{6}$$

The reduced damped equations of motion can now be determined as

$$\tilde{\mathbf{M}}\ddot{\tilde{\mathbf{U}}} + \tilde{\mathbf{C}}\dot{\tilde{\mathbf{U}}} + \tilde{\mathbf{K}}\tilde{\mathbf{U}} = -\tilde{\mathbf{G}}\ddot{x}_g + \tilde{\mathbf{P}}\mathbf{f} \tag{7}$$

where $\tilde{\mathbf{U}}$ is the vector of the active DOFs remaining in the model after the Guyan reduction,

$$\begin{aligned} \tilde{\mathbf{M}} &= \mathbf{T}_G^T \hat{\mathbf{M}} \mathbf{T}_G, \qquad \tilde{\mathbf{K}} = \mathbf{T}_G^T \hat{\mathbf{K}} \mathbf{T}_G \\ \tilde{\mathbf{G}} &= \mathbf{T}_G^T \hat{\mathbf{G}}, \qquad \tilde{\mathbf{P}} = \mathbf{T}_G^T \hat{\mathbf{P}} \end{aligned} \tag{8}$$

and

$$\mathbf{T}_G = \begin{bmatrix} \mathbf{I} \\ \hat{\mathbf{T}}_{da} \end{bmatrix}, \qquad \hat{\mathbf{T}}_{da} = -\hat{\mathbf{K}}_{dd}^{-1} \hat{\mathbf{K}}_{da} \tag{9}$$

Again, $\hat{\mathbf{G}}$ and $\hat{\mathbf{P}}$ are reordered corresponding to the active and dependent DOFs prior to making the transformation in Eq. (8).

The damping matrix $\tilde{\mathbf{C}}$ is defined based on the reduced system and the assumption of modal damping. Damping in each mode is assumed to be proportional to the mode's associated frequency, with a maximum of 10% critical damping in any one mode. The damping in the first mode is assumed to be 2%; therefore the damping ζ_i in the *i*th mode is given by

$$\zeta_i = \min\left\{ \frac{\omega_i}{50\omega_1}, 0.1 \right\} \tag{10}$$

where ω_i is the natural frequency of the *i*th mode. The damping matrix, $\tilde{\mathbf{C}}$ is then determined via

$$\tilde{\mathbf{C}} = \tilde{\mathbf{M}}\boldsymbol{\Phi}\begin{bmatrix} 2\zeta_1\omega_1 & 0 & 0 \\ 0 & \cdots & 0 \\ 0 & 0 & 2\zeta_n\omega_n \end{bmatrix}\boldsymbol{\Phi}^{-1} \tag{11}$$

where $\boldsymbol{\Phi}$ is the matrix of mode shapes (*i.e.*, the eigenvectors of $\tilde{\mathbf{M}}^{-1}\tilde{\mathbf{K}}$).

The Guyan reduction results in a final model with 106 DOFs, that maintains the important dynamics of the original model. The natural frequencies of the resulting model are less than 110 Hz.

A state space representation of the input-output model for the LA 20-story structure is now developed. The model is of the form

$$\dot{\mathbf{x}} = \mathbf{A}\mathbf{x} + \mathbf{B}\mathbf{f} + \mathbf{E}\ddot{x}_g \tag{12}$$

$$\mathbf{y}_m = \mathbf{C}_m\mathbf{x} + \mathbf{D}_m\mathbf{f} + \mathbf{F}_m\ddot{x}_g + \mathbf{v} \tag{13}$$

$$\mathbf{y}_e = \mathbf{C}_e\mathbf{x} + \mathbf{D}_e\mathbf{f} + \mathbf{F}_e\ddot{x}_g \tag{14}$$

$$\mathbf{y}_c = \mathbf{C}_c\mathbf{x} + \mathbf{D}_c\mathbf{f} + \mathbf{F}_c\ddot{x}_g \tag{15}$$

where $\mathbf{x} = [\tilde{\mathbf{U}}^T, \dot{\tilde{\mathbf{U}}}^T]^T$ is the state vector, $\mathbf{y}_m$ is the vector corresponding to the measured outputs, $\mathbf{v}$ is a measurement noise vector, $\mathbf{y}_e$ is the vector corresponding to the regulated outputs that are used for evaluation of the system, and $\mathbf{y}_c$ is the vector of output responses that are used as inputs to control device models. The coefficient matrices for Eq. (12) are given by

$$\mathbf{A} = \begin{bmatrix} \mathbf{0} & \mathbf{I} \\ -\tilde{\mathbf{M}}^{-1}\tilde{\mathbf{K}} & -\tilde{\mathbf{M}}^{-1}\tilde{\mathbf{C}} \end{bmatrix}, \quad \mathbf{B} = \begin{bmatrix} \mathbf{0} \\ \tilde{\mathbf{M}}^{-1}\tilde{\mathbf{P}} \end{bmatrix} \quad \mathbf{E} = \begin{bmatrix} \mathbf{0} \\ -\tilde{\mathbf{M}}^{-1}\tilde{\mathbf{G}} \end{bmatrix} \tag{16}$$

where $\mathbf{C}_m$, $\mathbf{C}_e$, $\mathbf{C}_c$, $\mathbf{D}_m$, $\mathbf{D}_e$, $\mathbf{D}_c$, $\mathbf{F}_m$, $\mathbf{F}_e$, and $\mathbf{F}_c$ are appropriately chosen matrices corresponding to the associated output vectors as defined by each designer/researcher. Specific examples of these matrices are given in the Sample Control System Design section.

The model of Eqs. (12–15) represents the input-output behavior of the LA 20-story structure considered for this study. The first 10 natural frequencies of this model are: 0.26, 0.75, 1.30, 1.83, 2.40, 2.80, 3.00, 3.21, 3.63 and 4.31 Hz. These results are consistent with those found by others who have modeled this structure. The first three mode shapes are given in Fig 4. Typical transfer functions for this structure comparing the reduced and full models are given in Fig. 5.

Degradation Effects

The change of the dynamic properties of a building from before (pre-earthquake) to after (post-earthquake) a strong motion earthquake can be substantial (Naeim 1997). This change can

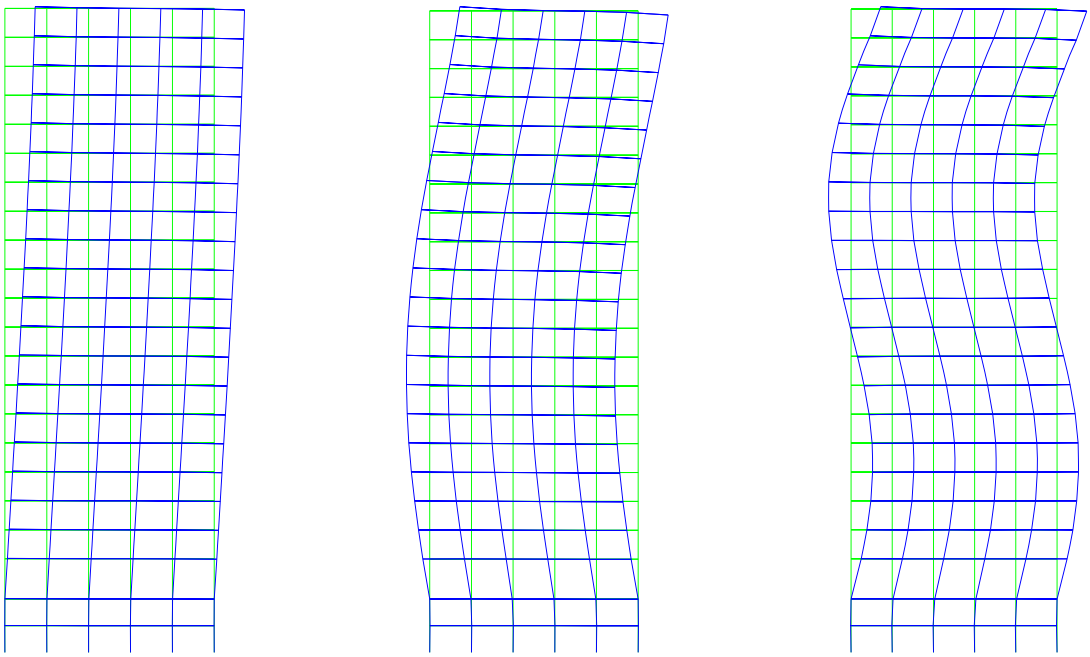

Figure 4: First Three Mode Shapes of the LA 20-story Building.

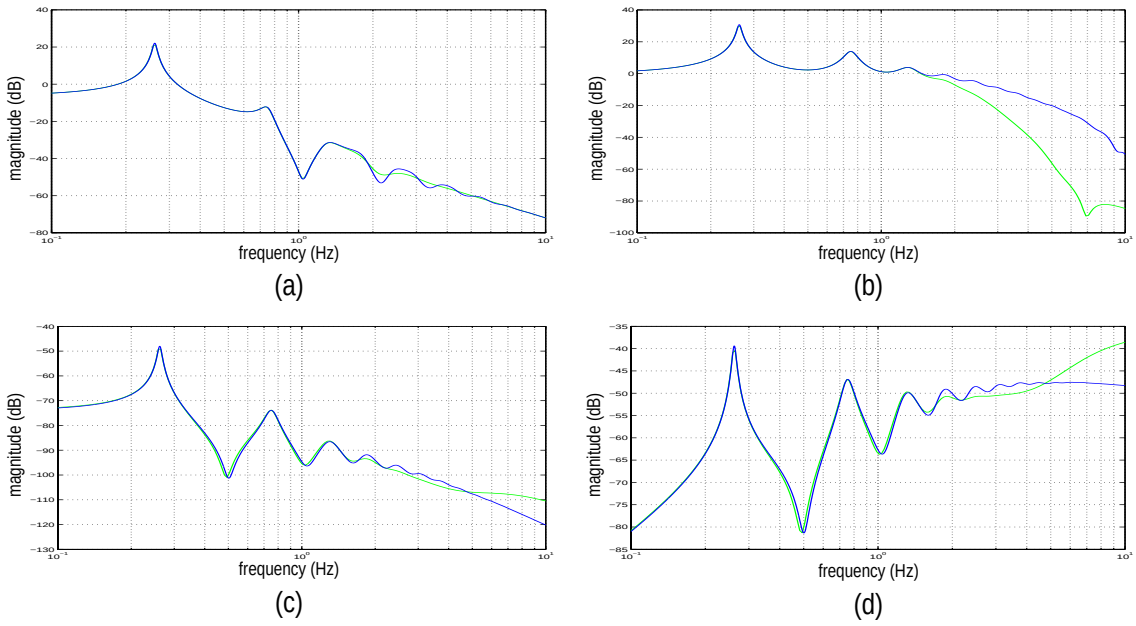

Figure 5: Typical Transfer Functions for the LA-20 Story Structure for the reduced (solid) and full (dotted) models. (a) ground excitation to roof horizontal displacement; (b) ground excitation to roof horizontal absolute acceleration; (c) horizontal force at roof to roof horizontal displacement; (d) horizontal force at roof to roof horizontal absolute acceleration (roof measurements taken at node-175).

cause as much as a 20% increase in the fundamental period, which is primarily due to stiffness degradation. Such stiffness reduction is attributed to the loss of non-structural elements and to damage of structural elements. Because the time between the main earthquake and subsequent significant aftershocks may not be large, an effective control system should be sufficiently robust to perform adequately based either on the pre-earthquake structure or the post-earthquake structure.

Two *evaluation* models are developed from the previously defined nominal structural model: the pre-earthquake evaluation model and the post-earthquake evaluation model. These two models are intended to account for the degradation effects that can occur within the structure during a strong ground motion and should be viewed as linearized models of the structure before and after degradation of the structure has occurred. The degradation of the benchmark building is modeled as a reduction in stiffness from the pre-earthquake to post-earthquake models. It should be noted that the post-earthquake building model assumes structural damage has occurred, which may be potentially avoided through the application of control device(s). Therefore, the post-earthquake building model may be viewed in some sense as representing a "worst-case" scenario.

The pre-earthquake evaluation model represents the LA 20-story structure as-built. The as-built structure includes additional stiffness provided by the lateral resistance of the structure's gravity system and non-structural elements such as partitions and cladding. The non-structural elements are accounted for in the pre-earthquake evaluation model by proportionally increasing the structural stiffness matrix such that the first natural frequency of the evaluation model is 10% greater than that of the nominal model. The pre-earthquake damping is determined, as indicated in Eq. (11), using this increased stiffness.

The post-earthquake evaluation model is intended to represent the LA 20-story structure after a strong motion earthquake. After a strong motion earthquake, the non-structural elements may no longer provide any additional stiffness to the structure. Moreover, the structural elements may be damaged, causing a decrease in stiffness. In this study, a post-earthquake evaluation model is developed in which the natural frequency of the structure is decreased by 10% from the nominal structural model. This reduction is accomplished by an associated reduction in the structural stiffness matrix, corresponding to an 18.2% reduction in natural frequency from the pre-earthquake evaluation model to the post-earthquake evaluation model. The post-earthquake damping is determined using this decreased stiffness.

The first 10 natural frequencies of the pre-earthquake model are: 0.29, 0.83, 1.43, 2.01, 2.64, 3.08, 3.30, 3.53, 3.99 and 4.74 Hz. The first 10 natural frequencies of the post-earthquake model are: 0.24, 0.68, 1.17, 1.65, 2.16, 2.52, 2.70, 2.89, 3.26 and 3.88 Hz. Typical transfer functions for the pre-earthquake and post-earthquake evaluation models, as compared to the nominal structural model, are given in Fig. 6. The pre-earthquake and post-earthquake evaluation models should be used to assess the performance of candidate control strategies and are considered for this study to be the true models of the structural system. Consequently, two values of the evaluation criteria, defined in the next section, should be reported for each control strategy, representing the performance with both the pre-earthquake structure and the post-earthquake structure.

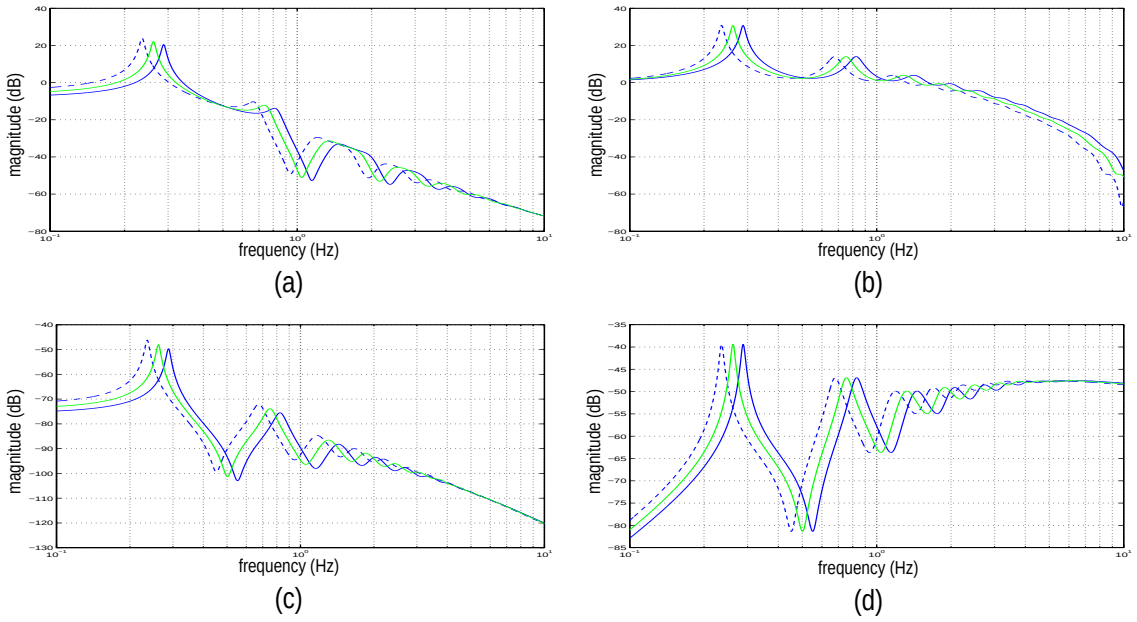

Figure 6: Typical Transfer Functions for the LA-20 Story Structure for the pre-earthquake (solid), post-earthquake (dashed) and original reduce (dotted) models. (a) ground excitation to roof horizontal displacement; (b) ground excitation to roof horizontal absolute acceleration; (c) horizontal force at roof to roof horizontal displacement; (d) horizontal force at roof to roof horizontal absolute acceleration (roof measurements taken at node-175).

Control Design Problem

The task of the designer/researcher in the benchmark study control design problem is to define an appropriate passive, active, or semi-active control strategy, or a combination thereof. It is left to the designer/researcher to define the type, appropriate model and location of the control device(s)/sensor(s) and to develop appropriate control algorithms. The evaluation model, however, will remain invariant to the various applied control strategy. By using a single building model and common evaluation criteria, various control strategies can be compared directly to one another.

Interfacing with the Evaluation Model

To interface with the benchmark building model defined in Eqs. (12–15), the outputs of the evaluation model must be measured by sensors. Researchers/designers must develop models for the sensors which take the following form

$$\dot{\mathbf{x}}^s = \mathbf{g}_1(\mathbf{x}^s, \mathbf{y}_m, \mathbf{f}_m, t) \tag{17}$$

$$\mathbf{y}^s = \mathbf{g}_2(\mathbf{x}^s, \mathbf{y}_m, \mathbf{f}_m, t) \tag{18}$$

where $\mathbf{x}^s$ is the continuous time state vector of the sensor(s), $\mathbf{f}_m$ is the continuous time vector of measured responses of the control device(s) (*i.e.*, which may include forces produced by individual control devices, device displacement, device acceleration, *etc*.), and $\mathbf{y}^s$ is the continuous time output of the sensor(s). All measured responses have units of Volts.

For active/semi-active control systems, the corresponding control algorithm must take the form

$$\mathbf{x}_{k+1}^c = \mathbf{g}_3(\mathbf{x}_k^c, \mathbf{y}_k^s, k) \tag{19}$$

$$\mathbf{u}_k = \mathbf{g}_4(\mathbf{x}_k^c, \mathbf{y}_k^s, k) \tag{20}$$

where $\mathbf{x}_k^c$ is the discrete state vector of the control algorithm at time $t = kT$, $\mathbf{y}_k^s$ is the sampled input to the control algorithm (discretized measured output from the sensor model), and $\mathbf{u}_k$ is the discrete control command from the control algorithm.

To interface with the benchmark building model defined in Eqs. (12–15) the control device model(s) must take the form

$$\dot{\mathbf{x}}^a = \mathbf{g}_5(\mathbf{x}^a, \mathbf{y}_c, \mathbf{u}_k, t) \tag{21}$$

$$\mathbf{f} = \mathbf{g}_6(\mathbf{x}^a, \mathbf{y}_c, \mathbf{u}_k, t) \tag{22}$$

$$\mathbf{f}_m = \mathbf{g}_7(\mathbf{x}^a, \mathbf{y}_c, \mathbf{u}_k, t) \tag{23}$$

$$\mathbf{y}_f = \mathbf{g}_8(\mathbf{x}^a, \mathbf{y}_c, \mathbf{u}_k, t) \tag{24}$$

where $\mathbf{x}^a$ is the continuous time state vector of the control device, $\mathbf{y}_c$ is the continuous time output from the evaluation model needed to evaluate the dynamics of the control devices, $\mathbf{f}$ is the continuous time force output of the control device(s) applied to the structure in units of (kN), and $\mathbf{y}_f$ is the vector of control device responses used for evaluation purposes. Note that for passive control devices, $\mathbf{g}_5$, $\mathbf{g}_6$, $\mathbf{g}_7$, $\mathbf{g}_8$ will not be a function of $\mathbf{u}_k$.

The SIMULINK model to be employed in performance evaluation is shown in Fig. 7.

Evaluation Criteria

In evaluating proposed control strategies, the input excitation $\ddot{x}_g$ (m/sec^2) is assumed to be one of the four historical earthquake records: (i) *El Centro*. The N-S component recorded at the Imperial Valley Irrigation District substation in El Centro, California, during the Imperial Valley, California earthquake of May, 18, 1940. (ii) *Hachinohe*. The N-S component recorded at Hachinohe City during the Takochi-oki earthquake of May, 16, 1968. (iii) *Northridge*. The N-S component recorded at Sylmar County Hospital parking lot in Sylmar, California, during the Northridge, California earthquake of January 17, 1994. (iv) *Kobe*. The N-S component recorded at the Kobe

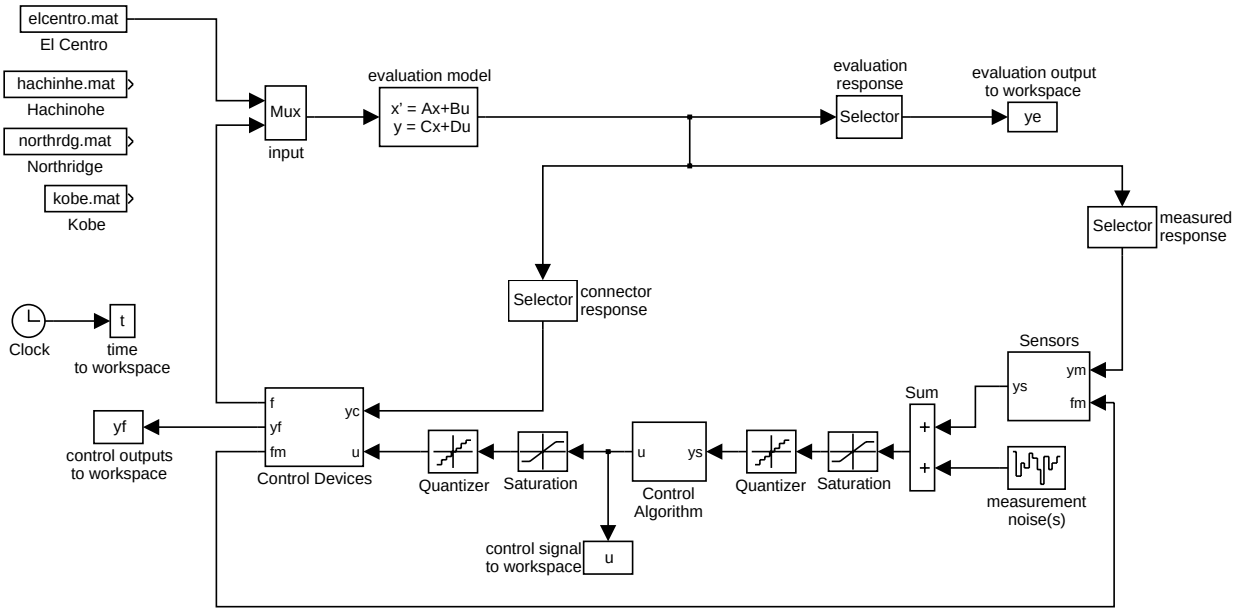

Figure 7: SIMULINK Model for Benchmark Problem.

Japanese Meteorological Agency (JMA) station during the Hyogo-ken Nanbu earthquake of January 17, 1995. Each proposed control strategy should be evaluated for all four earthquake records, with the appropriate responses being used to calculate the evaluation criteria for both the pre-earthquake and post-earthquake evaluation models. As detailed in the following paragraphs, the merit of a control strategy is based on criteria given in terms of maximum response quantities, as well as the number of sensors and control devices and the total power required by the control system. Smaller values of these evaluation criteria are generally more desirable.

The first evaluation criterion is a non-dimensionalized measure of the floor displacement relative to the ground, which is given as

$$J_1 = \max_{\substack{\text{El Centro}\\ \text{Hachinohe}\\ \text{Northridge}\\ \text{Kobe}}} \left\{ \frac{\max\limits_{i \in \boldsymbol{\eta}}^{t} \left| x_i(t) \right|}{x^{\max}} \right\} \tag{25}$$

where $\boldsymbol{\eta}$ = {8, 17, 20, 23, 32, 35, 38, 47, 50, 53, 62, 65, 68, 77, 80, 83, 92, 95, 104, 107} represents the set of states corresponding to the horizontal displacement of above ground floors (*i.e.*, nodes 21, 33, 39, 45, 57, 63, 69, 81, 87, 93, 105, 111, 117, 129, 135, 141, 153, 159, 171, 177, respectively, which are located on the third column line from the south on the N-S MRF) relative to the ground as given in terms of the states in Eq. (12), $x_i(t)$ is the time history of the ith state, $x^{\max}$ is the maximum uncontrolled displacement, and $|\cdot|$ denotes absolute value. Note that these responses correspond to each respective earthquake. Values for $x^{\max}$, as well as other uncontrolled responses required for the evaluation criteria, are given at the end of this section.

For each earthquake, the maximum drifts are non-dimensionalized and normalized with respect to the associated floor height (*i.e.*, the drift ratios). Therefore, the second evaluation criterion is given by

$$J_2 = \max_{\substack{\text{El Centro}\\ \text{Hachinohe}\\ \text{Northridge}\\ \text{Kobe}}} \left\{ \frac{\max\limits_{t,\,i} \dfrac{|d_i(t)|}{h_i}}{d_{\mathrm{n}}^{\max}} \right\} \tag{26}$$

where $d_i(t)$ is the interstory drift of the above ground floors over the time history of each earthquake, h_i is the height of each of the associated stories ($h_1 = 5.49$ m; $h_i = 3.96$ m, $i = 2, \ldots, 20$), and $d_{\mathrm{n}}^{\max} = \max\limits_{i,t}\{d_i(t)/h_i\}$ is the uncontrolled maximum interstory drift ratio corresponding to each respective earthquake. The interstory drifts are given by $d_i(t) = x_{\eta_i}(t) - x_{\eta_{i-1}}(t)$ where it is assumed $x_{\eta_0} \equiv 0$. Note that the interstory drifts are determined using the nodes on the third column line from the south, as were the displacements.

The third evaluation criterion is given in terms of the maximum floor accelerations, yielding

$$J_3 = \max_{\substack{\text{El Centro}\\ \text{Hachinohe}\\ \text{Northridge}\\ \text{Kobe}}} \left\{ \frac{\max\limits_{\substack{t\\ i \in \boldsymbol{\eta}}} |\ddot{x}_{\mathrm{a}i}(t)|}{\ddot{x}_{\mathrm{a}}^{\max}} \right\} \tag{27}$$

where the absolute accelerations of the ith state, $\ddot{x}_{\mathrm{a}i}(t)$, are non-dimensionalized by the maximum uncontrolled floor acceleration, denoted $\ddot{x}_{\mathrm{a}}^{\max}$, corresponding respectively to each earthquake.

The non-dimensionalized base shear is used as the fourth evaluation criterion such that

$$J_4 = \max_{\substack{\text{El Centro}\\ \text{Hachinohe}\\ \text{Northridge}\\ \text{Kobe}}} \left\{ \frac{\max\limits_{t} \left| \sum\limits_{i=1}^{20} m_i \ddot{x}_{\mathrm{a}\eta_i}(t) \right|}{F_b^{\max}} \right\} \tag{28}$$

where m_i is the seismic mass of each of the above-ground floors of a single N-S MRF ($m_1 = 2.83\times10^5$ kg; $m_i = 2.76\times10^5$ kg, $i = 2, \ldots, 19$; $m_{20} = 2.92\times10^5$ kg), $F_b^{\max}$ is the maximum uncontrolled base shear for each respective earthquake. Note that m_1 refers to the seismic mass of the first above-ground floor, which corresponds to the second level of the structure and that m_{20} refers to the seismic mass of the 20th above-ground floor, which corresponds to the roof of the structure, with all other ith above-ground floors corresponding to the $i + 1$ level of the structure.

To obtain insight into the performance of the controlled structural system that may not be provided by the maximum response evaluation criteria, four evaluation criteria correspond to L_2-

normed measures of the structural responses are considered. Therefore, the fifth evaluation criterion is a normed/non-dimensionalized measure of the maximum floor displacement of the building relative to the ground, which is given as

$$J_5 = \max_{\substack{\text{El Centro}\\ \text{Hachinohe}\\ \text{Northridge}\\ \text{Kobe}}} \left\{ \frac{\max_{i \in \boldsymbol{\eta}} \left\| x_i(t) \right\|}{\left\| x^{\max} \right\|} \right\} \tag{29}$$

where $\left\| x_i(t) \right\| \equiv \sqrt{\int_0^{t_f} x_i^2(t)\,dt}$, t_f is a sufficiently large time to allow the response of the structure to attenuate to less than 0.1% of its maximum value, and $\left\| x^{\max} \right\| \equiv \max_{i \in \boldsymbol{\eta}} \left\| x_i(t) \right\|$ is the maximum normed uncontrolled displacement for each of the respective earthquakes.

The sixth evaluation criterion provides a normed measure of the maximum drift ratios and is given by

$$J_6 = \max_{\substack{\text{El Centro}\\ \text{Hachinohe}\\ \text{Northridge}\\ \text{Kobe}}} \left\{ \frac{\max_{t,\,i} \dfrac{\left\| d_i(t) \right\|}{h_i}}{\left\| d_{\mathrm{n}}^{\max} \right\|} \right\} \tag{30}$$

where $\left\| d_{\mathrm{n}}^{\max} \right\| \equiv \max_{i \in \boldsymbol{\eta}} \left\| d_i(t) \right\|$ is the maximum normed interstory drift ratio corresponding to the uncontrolled structure excited by each respective earthquake.

The seventh evaluation criterion is given in terms of the normed floor accelerations, yielding

$$J_7 = \max_{\substack{\text{El Centro}\\ \text{Hachinohe}\\ \text{Northridge}\\ \text{Kobe}}} \left\{ \frac{\max_{i \in \boldsymbol{\eta}} \left\| \ddot{x}_{\mathrm{a}i}(t) \right\|}{\left\| \ddot{x}_{\mathrm{a}}^{\max} \right\|} \right\} \tag{31}$$

where $\left\| \ddot{x}_{\mathrm{a}}^{\max} \right\| \equiv \max_{i \in \boldsymbol{\eta}} \left\| \ddot{x}_{\mathrm{a}i}(t) \right\|$ is the maximum normed absolute acceleration of the uncontrolled structure excited by each respective earthquake.

The normed/non-dimensionalized base shear is used as the eighth evaluation criterion such that

$$J_8 = \max_{\substack{\text{El Centro}\\ \text{Hachinohe}\\ \text{Northridge}\\ \text{Kobe}}} \left\{ \frac{\left\| \sum_{i=1}^{20} m_i \ddot{x}_{\mathrm{a}\eta_i}(t) \right\|}{\left\| F_b^{\max} \right\|} \right\} \tag{32}$$

where $\left\| F_b^{\max} \right\| \equiv \max_{i \in \boldsymbol{\eta}} \left\| \sum_{i=1}^{20} m_i \ddot{x}_{a\eta_i}(t) \right\|$ is the maximum normed uncontrolled base shear for each respective earthquake.

The remaining evaluation criteria deal with the specified control system. Evaluation criterion nine considers the maximum required control force and is described as

$$J_9 = \max_{\substack{\text{El Centro} \\ \text{Hachinohe} \\ \text{Northridge} \\ \text{Kobe}}} \left\{ \frac{\max_{t,i} \left| f^i(t) \right|}{W} \right\} \tag{33}$$

where $f^i(t)$ is the force generated by the *i*th control device over the time history of each earthquake (note this is not the *i*th component of the $\mathbf{f}$ vector, which would correspond to the force at the *i*th control input, but is the force of the *i*th control device), and $W = 54,377$ kN (12,225 kips) is the seismic weight of the N-S MRF being controlled based on the above ground mass of the structure (excluding the mass of the 1st level).

The tenth criterion is based on the maximum displacement of the control devices. This performance measure is given as

$$J_{10} = \max_{\substack{\text{El Centro} \\ \text{Hachinohe} \\ \text{Northridge} \\ \text{Kobe}}} \left\{ \frac{\max_{t,i} \left| y_i^a(t) \right|}{x^{\max}} \right\} \tag{34}$$

where $y_i^a(t)$ is the displacement of the *i*th control device over the time histories of each earthquake. For devices without an associated displacement (*e.g.,* tuned liquid dampers), this evaluation constraint is zero.

The eleventh evaluation criterion is a measure of the maximum power required to control the structure and is defined as

$$J_{11} = \max_{\substack{\text{El Centro} \\ \text{Hachinohe} \\ \text{Northridge} \\ \text{Kobe}}} \left\{ \frac{\max_{t} \left[\sum_i \mathcal{P}_i(t) \right]}{\dot{x}^{\max} W} \right\} \tag{35}$$

where $\mathcal{P}_i(t)$ is a measure of the instantaneous power required by the *i*th control device, and $\dot{x}^{\max}$ is the maximum uncontrolled velocity of the floors relative to the ground. For active control devices, $\mathcal{P}_i(t) \equiv \left| \dot{y}_i^a(t) f^i(t) \right|$, where $\dot{y}_i^a(t)$ is the velocity of the *i*th control device. For semi-active devices, $\mathcal{P}_i(t)$ is the actual power required to operate the device. For passive control devices, this criterion is zero.

The twelfth evaluation criterion is a measure of the total power required for the control of the structure, which is defined as

$$J_{12} = \max_{\substack{\text{El Centro}\\ \text{Hachinohe}\\ \text{Northridge}\\ \text{Kobe}}} \left\{ \frac{\sum_i \left\| \mathcal{P}_i(t) \right\|}{x^{\max} W} \right\} \tag{36}$$

For passive control devices, the criterion J_{12} is zero.

The thirteenth evaluation criterion is a measure of the total number of control devices required in the control system to control one of the N-S MRFs of the structure.

$$J_{13} = \text{number of control devices required} \tag{37}$$

The fourteenth evaluation criterion is a measure of the total number of sensors required in the control system to control one of the N-S MRFs of the structure.

$$J_{14} = \text{number of sensors required} \tag{38}$$

A final evaluation criterion provides a measure of the computational resources required to implement the control algorithm and is given by

$$J_{15} = \dim(\mathbf{x}_k^c) \tag{39}$$

where $\mathbf{x}_k^c$ is the discrete state vector of the control algorithm given in Eq. (19).

The maximum uncontrolled responses for the four earthquakes are given Table 1. A summary of the fifteen evaluation criteria are given in Table 2. All fifteen criteria should be reported for each proposed control strategy implemented in both the pre-earthquake and post-earthquake models. The El Centro, Hachinohe, Northridge and Kobe earthquakes should all be considered in determining the evaluation criteria.

Designers/researchers are also encouraged to include other criteria in their results if, through these criteria, important features of their control strategy can be demonstrated. For example, the performance of nonlinear control systems may substantially vary with the amplitude of the disturbance. Therefore, examining the performance of such control strategies subject to several different levels of ground motion may be warranted.

Control Implementation Constraints and Procedures

To make the benchmark problem as representative of the full-scale implementation as possible and to allow for direct comparison of the results submitted to the study, the following constraints and procedures are specified:

1. The measured outputs directly available for use in determination of the control action are the absolute horizontal acceleration and the interstory drift of each floor of the LA 20-story structure, and control device outputs which are readily available (*e.g.*, control device displacement,

Table 1: Uncontrolled Peak Response Quantities of the Pre- and Post-Earthquake Evaluation Models.

	El Centro		Hachinohe		Northridge		Kobe	
	pre-earthquake	post-earthquake	pre-earthquake	post-earthquake	pre-earthquake	post-earthquake	pre-earthquake	post-earthquake
$x^{\max}$ (m)	0.37959	0.27787	0.51705	0.29831	1.0591	0.90765	0.56887	0.65617
$\dot{x}^{\max}$ (m/sec)	0.82539	0.74801	1.0450	0.76065	2.9023	2.6803	1.8370	1.6289
$\ddot{x}_{\mathrm{a}}^{\max}$ (m/sec^2)	3.1372	2.8093	2.8439	1.9467	9.1886	7.7702	8.9544	7.7383
$d_{\mathrm{n}}^{\max}$	6.2297 x10^{-3}	4.8655 x10^{-3}	7.6232 x10^{-3}	5.4667 x10^{-3}	15.644 x10^{-3}	18.484 x10^{-3}	13.353 x10^{-3}	14.223 x10^{-3}
$F_b^{\max}$ (kN)	4.3525 x10^{6}	2.0892 x10^{6}	5.3852 x10^{6}	2.6514 x10^{6}	11.083 x10^{6}	8.0311 x10^{6}	9.4430 x10^{6}	6.2433 x10^{6}
$\lVert x^{\max} \rVert$ (m $\cdot \sqrt{\text{sec}}$)	0.80902	0.89099	1.4934	1.0881	2.4997	1.6861	0.99073	2.3438
$\lVert \ddot{x}_{\mathrm{a}}^{\max} \rVert$ (m $\cdot$ sec$^{-3/2}$)	4.7166	3.5697	5.7325	3.2852	10.329	8.8355	9.8980	9.5907
$\lVert d_{\mathrm{n}}^{\max} \rVert$ ($\sqrt{\text{sec}}$)	1.2486 x10^{-2}	1.3707 x10^{-2}	2.2026 x10^{-2}	1.5781 x10^{-2}	3.7074 x10^{-2}	2.8271 x10^{-2}	1.7807 x10^{-2}	3.7656 x10^{-2}
$\lVert F_b^{\max} \rVert$ (kN $\cdot \sqrt{\text{sec}}$)	8.8861 x10^{6}	6.5488 x10^{6}	15.5564 x10^{6}	7.4806 x10^{6}	26.247 x10^{6}	13.464 x10^{6}	12.913 x10^{6}	17.986 x10^{6}

force, or absolute acceleration). Although absolute velocity measurements are not available, they can be closely approximated by passing the measured accelerations through a second order filter as described in Spencer, *et al*. (1998).

2. The digitally implemented controller has a sampling time of $T = 0.005$ sec.

3. The A/D and D/A converters on the digital controller have 12-bit precision and a span of ±10 Volts.

4. Each of the measured responses contains an RMS noise of 0.03 Volts, which is approximately 0.3% of the full span of the A/D converters. The measurement noises are modeled as Gaussian rectangular pulse processes with a pulse width of 0.001 seconds.

Table 2: Summary of Evaluation Criteria for the Benchmark Problem.

Floor Displacement $J_1 = \max_{\substack{\text{El Centro}\\\text{Hachinohe}\\\text{Northridge}\\\text{Kobe}}} \left\{ \frac{\max_t \lvert x_i(t) \rvert}{x^{\max}} \right\}$	Normed Floor Displacement $J_5 = \max_{\substack{\text{El Centro}\\\text{Hachinohe}\\\text{Northridge}\\\text{Kobe}}} \left\{ \frac{\max_{i \in \boldsymbol{\eta}} \lVert x_i(t) \rVert}{\lVert x^{\max} \rVert} \right\}$	Control Force $J_9 = \max_{\substack{\text{El Centro}\\\text{Hachinohe}\\\text{Northridge}\\\text{Kobe}}} \left\{ \frac{\max_{t,i} \lvert f^i(t) \rvert}{W} \right\}$	Control Devices J_{13} = number of control devices required
Interstory Drift $J_2 = \max_{\substack{\text{El Centro}\\\text{Hachinohe}\\\text{Northridge}\\\text{Kobe}}} \left\{ \frac{\max_{t,i} \left(\frac{\lvert d_i(t) \rvert}{h_i} \right)}{d_{\text{n}}^{\max}} \right\}$	Normed Interstory Drift $J_6 = \max_{\substack{\text{El Centro}\\\text{Hachinohe}\\\text{Northridge}\\\text{Kobe}}} \left\{ \frac{\max_{t,i} \left(\frac{\lVert d_i(t) \rVert}{h_i} \right)}{\lVert d_{\text{n}}^{\max} \rVert} \right\}$	Control Device Stroke $J_{10} = \max_{\substack{\text{El Centro}\\\text{Hachinohe}\\\text{Northridge}\\\text{Kobe}}} \left\{ \frac{\max_{t,i} \lvert y_i^{\text{a}}(t) \rvert}{x^{\max}} \right\}$	Sensors J_{14} = number of sensors required
Floor Acceleration $J_3 = \max_{\substack{\text{El Centro}\\\text{Hachinohe}\\\text{Northridge}\\\text{Kobe}}} \left\{ \frac{\max_t \lvert \ddot{x}_{\text{a}i}(t) \rvert}{\ddot{x}_{\text{a}}^{\max}} \right\}$	Normed Floor Acceleration $J_7 = \max_{\substack{\text{El Centro}\\\text{Hachinohe}\\\text{Northridge}\\\text{Kobe}}} \left\{ \frac{\max_{i \in \boldsymbol{\eta}} \lVert \ddot{x}_{\text{a}i}(t) \rVert}{\lVert \ddot{x}_{\text{a}}^{\max} \rVert} \right\}$	Control Power $J_{11} = \max_{\substack{\text{El Centro}\\\text{Hachinohe}\\\text{Northridge}\\\text{Kobe}}} \left\{ \frac{\max_t \left[\sum_i \mathcal{P}_i(t) \right]}{\dot{x}^{\max} W} \right\}$	Computational Resources $J_{15} = \dim(\mathbf{x}_k^{\text{c}})$
Base Shear $J_4 = \max_{\substack{\text{El Centro}\\\text{Hachinohe}\\\text{Northridge}\\\text{Kobe}}} \left\{ \frac{\max_t \left\lvert \sum_{i=1}^{20} m_i \ddot{x}_{\text{a}\eta_i}(t) \right\rvert}{F_b^{\max}} \right\}$	Normed Base Shear $J_8 = \max_{\substack{\text{El Centro}\\\text{Hachinohe}\\\text{Northridge}\\\text{Kobe}}} \left\{ \frac{\left\lVert \sum_{i=1}^{20} m_i \ddot{x}_{\text{a}\eta_i}(t) \right\rVert}{\lVert F_b^{\max} \rVert} \right\}$	Normed Control Power $J_{12} = \max_{\substack{\text{El Centro}\\\text{Hachinohe}\\\text{Northridge}\\\text{Kobe}}} \left\{ \frac{\sum_i \lVert \mathcal{P}_i(t) \rVert}{\dot{x}^{\max} W} \right\}$	

5. No hard limit is placed on the number of states of the control algorithm, although the number of states should be kept to a reasonable number as limited computational resources in the digital controller exist. The designer/researcher should justify that the proposed algorithm(s) can be implemented with currently available computing hardware.

6. The control algorithm is required to be stable.

7. The performance of each control design should be evaluated using both the 212 state pre-earthquake evaluation model and the 212 state post-earthquake evaluation model for each of the earthquake records provided (*i.e.*, El Centro, Hachinohe, Northridge and Kobe).

8. The closed loop stability robustness for each proposed active control design should be discussed.

9. The control signal to each control device has a constraint of $\max_t \left|u_i(t)\right| \leq 10$ Volts for each respective earthquake.

10. The capabilities of each control device employed should be discussed, and the designer/researcher should provide a justification of the availability of each control device. Additional constraints unique to each control scheme should also be reported (*e.g.*, maximum displacement, velocity, or force capacity of control devices).

11. Designers/researchers should submit electronically a complete set of MATLAB files that will produce the evaluation criteria specified in this problem statement for both the pre- and post-earthquake evaluation models. For more details, see the *README* file included with the downloaded benchmark data on the benchmark homepage (*http://www.nd.edu/~quake/*).

Sample Control System Design

To illustrate some of the constraints and challenges of this benchmark problem, a sample control system is presented. The sample control system design is included to serve as a guide to the participants in this study and is not intended to be a competitive design. The sample control system is a type of active system that employs hydraulic actuators as control devices. Hydraulic actuators are located on each floor of the structure to provide control forces to the building. Feedback measurements are provided by accelerometers placed at various locations on the structure. In this section, the accelerometers and hydraulic actuators chosen for the sample control system are described, and models for each are discussed. A linear quadratic Gaussian (LQG) control algorithm is designed based on a reduced order model of the system. The results are then discussed and the evaluation criteria are then determined for both the pre-earthquake and post-earthquake evaluation models.

Sensors

Because accelerometers can readily provide reliable and inexpensive measurements of the absolute accelerations of arbitrary points on a structure, the sample control system is based on acceleration feedback. A total of five acceleration measurements were selected for feedback in the control system (on floors 5, 9, 13, 17 and the roof).

A wide variety of accelerometers are available, many with a natural frequency at least an order of magnitude above the dynamics of this structure. Thus, each accelerometer is modeled as having a constant magnitude and phase. The magnitude of the output of each accelerometer is 10 V / g (where $1g$ = 9.81 m/sec^2), which is the sensitivity of the sensor. Thus, in the form of Eqs. (17–18) the sensors can be modeled with $\mathbf{g}_1 = \mathbf{0}$ and

$$\mathbf{y}^{\mathrm{s}} = \mathbf{D}_{\mathrm{s}}\, \mathbf{y}_{\mathrm{m}} \tag{40}$$

where $\mathbf{D}_{\mathrm{s}} = (10/9.81)[\mathbf{I}]$ V / (m/sec^2). Based on the measurements selected for feedback in the sample control strategy, $\mathbf{y}_{\mathrm{m}} = [\ddot{x}_{a\eta_4}\ \ddot{x}_{a\eta_8}\ \ddot{x}_{a\eta_{12}}\ \ddot{x}_{a\eta_{16}}\ \ddot{x}_{a\eta_{20}}]^{\mathrm{T}}$.

For simulation purposes, the sensor block shown in Fig. 8 was used to represent the five accelerometers used in the sample control system design.

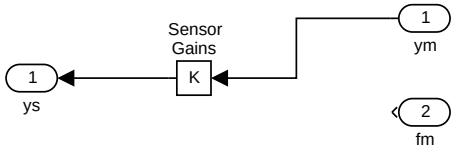

Figure 8: SIMULINK Block Representing the Sensors in the Sample Control System Design.

Control Devices

Hydraulic actuators are employed as the active control devices. The actuators are placed on each floor of the structure, and a total of 50 hydraulic actuators are used to control the N-S MRF in the sample control strategy. Eight actuators are located on the first floor, four actuators are located on both the second and third floors, and two actuators are on each of the remaining floors of the structure. Each actuator is implemented in the structure using a chevron brace configuration, in which the actuator is horizontal and rigidly attached between the two consecutive floors of the building. Thus, in the analysis the compliance of the bracing is neglected.

Using the model of a hydraulic actuator discussed in (Dyke, *et al*. 1995), the governing equation for the *i*th hydraulic actuator with position feedback is

$$\dot{f}^{i} = \frac{2\beta}{V}(Ak_q\gamma(u_i - y_i^{\mathrm{a}}) - k_c f^{i} - A^2 \dot{y}_i^{\mathrm{a}}), \tag{41}$$

where A is the cross-sectional area of the actuator, β is the bulk modulus of the fluid, V is the characteristic hydraulic fluid volume for the actuator, u_i is the command signal to the *i*th actuator, f^i is the force generated by the *i*th actuator, y_i^{a} is the displacement of the *i*th actuator, k_q, k_c are system constants, and γ is the proportional feedback gain stabilizing the actuator. Equation (41) can be rewritten as

$$\dot{f}^{i} = a_1 u_i - a_1 y_i^{\mathrm{a}} - a_2 \dot{y}_i^{\mathrm{a}} - a_3 f^{i} \tag{42}$$

where $a_1 = 2\beta k_q A/V$, $a_2 = 2\beta A^2/V$, $a_3 = 2\beta k_c/V$. The sample control system employs hydraulic actuators with a capacity of 897 kN (200 kips) and a stroke of ±8.9 cm (±3.5 in). To achieve this capacity, the actuator discussed in (Dyke, *et al.* 1995) was scaled up, and the resulting

values of the actuator parameters are $a_1 = 5.8128784 \times 10^6$ kN/m-sec, $a_2 = 5.4641931 \times 10^4$ kN/m, $a_3 = 1.6210740 \times 10^3$ sec^{-1}. Hydraulic actuators with these capabilities are readily available (*e.g.*, from IST[6] Systems or MTS[7]).

Because the control devices are oriented horizontally and assumed to be rigidly secured between two floors, the displacement of each control device is equal to the interstory drift of the level on which it is located. Thus the relationship between the displacements of the control devices and the displacements of the floors of the structure relative to the ground is

$$y_i^a(t) = d_i(t) = x_{\eta_i}(t) - x_{\eta_{i-1}}(t) \tag{43}$$

where $x_{\eta_0} = 0$. Using Eq. (43), the vector of control device displacements (which correspond to the interstory drifts of the structure), $\mathbf{y}^a$, can be determined from the vector of horizontal floor displacements relative to the ground, $\mathbf{x}_\eta = [\, x_{\eta_1}\ x_{\eta_2}\ \ldots\ x_{\eta_{20}}\,]^T$, using the transformation

$$\mathbf{y}^a = \mathbf{\Delta}\, \mathbf{x}_\eta \tag{44}$$

where

$$\mathbf{\Delta} = \begin{bmatrix} 1 & 0 & 0 & \cdots & 0 \\ -1 & 1 & 0 & \cdots & 0 \\ 0 & & \cdots & & \vdots \\ 0 & \cdots & & -1 & 1 & 0 \\ 0 & \cdots & & 0 & -1 & 1 \end{bmatrix}. \tag{45}$$

Although there are multiple control devices acting on each floor, it is assumed that all of the actuators on a single floor experience the same inputs, and respond in the same way. Thus, only twenty independent equations (and states) are needed to fully describe the dynamics of the fifty actuators. From Eq. (42) a single state space equation is formed to describe the dynamics of the hydraulic actuators on all twenty floors in the form of Eqs. (21-24), as

$$\dot{\mathbf{x}}^a = \mathbf{A}_a \mathbf{x}^a + \mathbf{B}_a \begin{bmatrix} \mathbf{u} \\ \mathbf{y}_c \end{bmatrix} \tag{46}$$

$$\mathbf{f} = \mathbf{C}_a \mathbf{x}^a + \mathbf{D}_a \begin{bmatrix} \mathbf{u} \\ \mathbf{y}_c \end{bmatrix} \tag{47}$$

---

6. IST Systems, 2890 John R Road, Troy, MI 48083.
7. MTS Systems Corporation, 14000 Technology Drive, Eden Prarie, MN 55344-2290.

where the state vector $\mathbf{x}^a$ corresponds to the vector of forces provided by one control device for each floor (*e.g.*, x_1^a is the force generated by each of the eight control actuators on the first floor), $\mathbf{u}$ is the control input to each actuator, $\mathbf{y}_c = [\, \mathbf{x}_{\boldsymbol{\eta}}^T \;\; \dot{\mathbf{x}}_{\boldsymbol{\eta}}^T \,]^T$ is the specific connector output required for the hydraulic actuator including the relative horizontal displacements and velocities of each floor, and $\mathbf{f}$ is the vector of forces applied to the structure. For the sample system, the vector of control device responses used for evaluation is $\mathbf{y}_f = \mathbf{f}$, and no control device outputs are used for feedback (*i.e.*, $\mathbf{f}_m = [\,]$). The coefficient matrices for Eq. (46) are given by

$$\mathbf{A}_a = \left[-a_3\mathbf{I}\right], \qquad \mathbf{B}_a = \left[a_1\mathbf{I} \;\middle|\; -a_1\boldsymbol{\Delta} \;\middle|\; -a_2\boldsymbol{\Delta}\right] \tag{48}$$

In Eq. (47), $\mathbf{C}_a$ is a diagonal $[20 \times 20]$ matrix with the number of actuators per floor on the diagonals, and $\mathbf{D}_a$ is a $[20 \times 60]$ matrix of zeros.

The SIMULINK block shown in Fig. 9 is used to represent the control devices for the sample control system design in the simulation. Here, to facilitate recording of the individual control forces required for calculation of the evaluation criteria (*i.e.*, $\mathbf{y}_f$), the response of each of the independent control devices is output from the 'state space' block, and the 'Matrix gain' block is used to account for multiple devices acting on a single floor. Notice that this design only makes use of the absolute accelerations of five floors of the structure, although additional measurements are available for feedback.

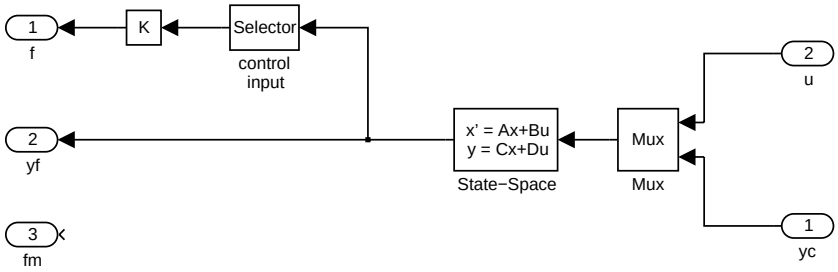

Figure 9: SIMULINK Block Representing the Control Devices in the Sample Control System Design.

Control Design Model

Because the evaluation model is quite large, a reduced order model of the system, designated the *design* model, is developed for purposes of control design. Previous experience with hydraulic control systems has shown that increased performance can be achieved when the dynamics of the control device are incorporated into the design model (Dyke, *et al.* 1995). Therefore, here a model reduction is first performed on the evaluation model, and then the actuator dynamics are appended to the reduced model to form the design model.

The reduced order model of the structure is given as

$$\dot{\mathbf{x}}^r = \mathbf{A}_r\mathbf{x}^r + \mathbf{B}_r\mathbf{f} + \mathbf{E}_r\ddot{x}_g \tag{49}$$

$$\mathbf{y}_{mr} = \mathbf{C}_{mr}\mathbf{x}^{r} + \mathbf{D}_{mr}\mathbf{f} + \mathbf{F}_{mr}\ddot{x}_g + \mathbf{v} \tag{50}$$

$$\mathbf{y}_{wr} = \mathbf{C}_{wr}\mathbf{x}^{r} + \mathbf{D}_{wr}\mathbf{f} + \mathbf{F}_{wr}\ddot{x}_g \tag{51}$$

$$\mathbf{y}_{cr} = \mathbf{C}_{cr}\mathbf{x}^{r} + \mathbf{D}_{cr}\mathbf{f} + \mathbf{F}_{cr}\ddot{x}_g \tag{52}$$

where $\mathbf{x}^{r}$ is the reduced state vector, $\mathbf{y}_{mr} = [\ddot{x}_{a\eta_4}\ \ddot{x}_{a\eta_8}\ \ddot{x}_{a\eta_{12}}\ \ddot{x}_{a\eta_{16}}\ \ddot{x}_{a\eta_{20}}]^{T}$ is the vector of measured responses, $\mathbf{y}_{wr} = [\ddot{x}_{a\eta_1}\ldots\ddot{x}_{a\eta_{20}}]^{T}$ is the vector of regulated responses, $\mathbf{y}_{cr} = [x_{\eta_1}\ldots x_{\eta_{20}}\ \dot{x}_{\eta_1}\ldots\dot{x}_{\eta_{20}}]^{T}$ is the vector of connection responses, and $\mathbf{A}_r$, $\mathbf{B}_r$, $\mathbf{E}_r$, $\mathbf{C}_{mr}$, $\mathbf{C}_{wr}$, $\mathbf{C}_{cr}$, $\mathbf{D}_{mr}$, $\mathbf{D}_{wr}$, $\mathbf{D}_{cr}$, $\mathbf{F}_{mr}$, $\mathbf{F}_{wr}$, and $\mathbf{F}_{cr}$ are the reduced order coefficient matrices.

The design model is formed by stacking the states of the reduced structural model and the actuator model, as in

$$\dot{\mathbf{x}}^{d} = \mathbf{A}_d\mathbf{x}^{d} + \mathbf{B}_d\mathbf{u} + \mathbf{E}_d\ddot{x}_g \tag{53}$$

$$\mathbf{y}_{md} = \mathbf{C}_{md}\mathbf{x}^{d} + \mathbf{D}_{md}\mathbf{u} + \mathbf{F}_{md}\ddot{x}_g + \mathbf{v} \tag{54}$$

$$\mathbf{y}_{wd} = \mathbf{C}_{wd}\mathbf{x}^{d} + \mathbf{D}_{wd}\mathbf{u} + \mathbf{F}_{wd}\ddot{x}_g + \mathbf{v} \tag{55}$$

where $\mathbf{x}^{d} = [\mathbf{x}^{rT}\ \ \mathbf{x}^{aT}]^{T}$ is the state vector for the design model. The associated coefficient matrices are

$$\mathbf{A}_d = \begin{bmatrix} \mathbf{A}_r & \mathbf{B}_r\mathbf{C}_a \\ \boldsymbol{\theta}\mathbf{C}_{cr} & \mathbf{A}_a + \boldsymbol{\theta}\mathbf{D}_{cr}\mathbf{C}_a \end{bmatrix},\ \mathbf{B}_d = \begin{bmatrix} \mathbf{0} \\ a_1\mathbf{I} \end{bmatrix},\ \mathbf{E}_d = \begin{bmatrix} \mathbf{E}_r \\ \boldsymbol{\theta}\mathbf{F}_{cr} \end{bmatrix} \tag{56}$$

$$\mathbf{C}_{md} = \begin{bmatrix} \mathbf{C}_{mr} & \mathbf{D}_{mr}\mathbf{C}_a \end{bmatrix},\ \mathbf{C}_{wd} = \begin{bmatrix} \mathbf{C}_{wr} & \mathbf{D}_{wr}\mathbf{C}_a \end{bmatrix} \tag{57}$$

$$\mathbf{D}_{md} = \mathbf{D}_{wd} = \mathbf{0}\ ,\ \mathbf{F}_{md} = \mathbf{F}_{mr}\ \mathbf{F}_{wd} = \mathbf{F}_{wr} \tag{58}$$

where $\boldsymbol{\theta} = \begin{bmatrix} -a_1\mathbf{D} & -a_2\mathbf{D} \end{bmatrix}$.

Control Algorithm

To illustrate some of the challenges of this benchmark problem, a sample linear quadratic Gaussian (LQG) control design is presented. To simplify design of the controller, $\ddot{x}_g$ is taken to be a stationary white noise, and an infinite horizon performance index is chosen that weights the accelerations of the floors, *i.e.*,

$$\hat{J} = \lim_{\tau \to \infty} \frac{1}{\tau} \mathrm{E}\left[\int_0^{\tau} \left\{ (\mathbf{C}_{\mathrm{wd}}\mathbf{x}^{\mathrm{d}} + \mathbf{D}_{\mathrm{wd}}\mathbf{u})^{\mathrm{T}} \mathbf{Q} (\mathbf{C}_{\mathrm{wd}}\mathbf{x}^{\mathrm{d}} + \mathbf{D}_{\mathrm{wd}}\mathbf{u}) + \mathbf{R}\mathbf{u}^2 \right\} dt \right] \tag{59}$$

where $\mathbf{R}$ is a $[20 \times 20]$ diagonal matrix with a 4 in the (1,1) position, and ones in the remaining diagonal positions, and the weighting matrix $\mathbf{Q}$ was chosen to be a $[20 \times 20]$ matrix with equal weighting placed on each of the floor accelerations (*i.e.*, $\mathbf{Q} = 3 \times 10^{-3}[\mathbf{I}]$). Further, the measurement noises are assumed to be identically distributed, statistically independent Gaussian white noise processes, and $S_{\ddot{x}_g \ddot{x}_g} / S_{v_i v_i} = \gamma = 25$.

The separation principle allows the control and estimation problems to be considered separately, yielding a control law of the form (Stengel 1986; Skelton 1988)

$$\mathbf{u} = -\underset{\sim}{\mathbf{K}} \hat{\mathbf{x}}^{\mathrm{d}} \tag{60}$$

where $\hat{\mathbf{x}}^{\mathrm{d}}$ is the Kalman Filter estimate of the state vector based on the reduced order model, including the actuator models. By the certainty equivalence principle (Stengel 1986; Skelton 1988), $\underset{\sim}{\mathbf{K}}$ is the full state feedback gain matrix for the deterministic regulator problem given by

$$\underset{\sim}{\mathbf{K}} = \tilde{\mathbf{R}}^{-1} (\tilde{\mathbf{N}} + \mathbf{B}_{\mathrm{d}}^{\mathrm{T}} \underset{\sim}{\mathbf{P}}) \tag{61}$$

where $\underset{\sim}{\mathbf{P}}$ is the solution of the algebraic Riccati equation given by

$$\mathbf{0} = \underset{\sim}{\mathbf{P}} \tilde{\mathbf{A}} + \tilde{\mathbf{A}}^{\mathrm{T}} \underset{\sim}{\mathbf{P}} - \underset{\sim}{\mathbf{P}} \mathbf{B}_{\mathrm{d}} \tilde{\mathbf{R}}^{-1} \mathbf{B}_{\mathrm{d}}^{\mathrm{T}} \underset{\sim}{\mathbf{P}} + \tilde{\mathbf{Q}} \tag{62}$$

and

$$\tilde{\mathbf{Q}} = \mathbf{C}_{\mathrm{wd}}^{\mathrm{T}} \mathbf{Q} \mathbf{C}_{\mathrm{wd}} - \tilde{\mathbf{N}} \tilde{\mathbf{R}}^{-1} \tilde{\mathbf{N}}^{\mathrm{T}} \tag{63}$$

$$\tilde{\mathbf{N}} = \mathbf{C}_{\mathrm{wd}}^{\mathrm{T}} \mathbf{Q} \mathbf{D}_{\mathrm{wd}} \tag{64}$$

$$\tilde{\mathbf{R}} = \mathbf{R} + \mathbf{D}_{\mathrm{wd}}^{\mathrm{T}} \mathbf{Q} \mathbf{D}_{\mathrm{wd}} \tag{65}$$

$$\tilde{\mathbf{A}} = \mathbf{A}_{\mathrm{d}} - \mathbf{B}_{\mathrm{d}} \tilde{\mathbf{R}}^{-1} \tilde{\mathbf{N}}^{\mathrm{T}} \tag{66}$$

Calculations to determine $\underset{\sim}{\mathbf{K}}$ were done using the MATLAB (1997) routine *lqry.m* within the control toolbox.

The Kalman Filter optimal estimator is given by

$$\dot{\hat{\mathbf{x}}}^{\mathrm{d}} = \mathbf{A}_{\mathrm{d}} \hat{\mathbf{x}}^{\mathrm{d}} + \mathbf{B}_{\mathrm{d}} \mathbf{u} + \mathbf{L} (\mathbf{y}_{\mathrm{m}} - \mathbf{C}_{\mathrm{md}} \hat{\mathbf{x}}^{\mathrm{d}} - \mathbf{D}_{\mathrm{md}} \mathbf{u}) \tag{67}$$

$$\mathbf{L} = [\underset{\sim}{\mathbf{R}}^{-1}(\gamma \mathbf{F}_{md}\mathbf{E}_d^T + \mathbf{C}_{md}\mathbf{S})]^T \tag{68}$$

where $\mathbf{S}$ is the solution of the algebraic Riccati equation given by

$$\mathbf{0} = \mathbf{S}\underset{\sim}{\mathbf{A}} + \underset{\sim}{\mathbf{A}}^T\mathbf{S} - \mathbf{S}\underset{\sim}{\mathbf{G}}\mathbf{S} + \underset{\sim}{\mathbf{H}} \tag{69}$$

and

$$\underset{\sim}{\mathbf{A}} = \mathbf{A}_d^T - \mathbf{C}_{md}^T\underset{\sim}{\mathbf{R}}^{-1}(\gamma \mathbf{F}_{md}\mathbf{E}_d^T) \tag{70}$$

$$\underset{\sim}{\mathbf{G}} = \mathbf{C}_{md}^T\underset{\sim}{\mathbf{R}}^{-1}\mathbf{C}_{md} \tag{71}$$

$$\underset{\sim}{\mathbf{H}} = \gamma \mathbf{E}_d\mathbf{E}_d^T - \gamma^2\mathbf{E}_d\mathbf{F}_{md}^T\underset{\sim}{\mathbf{R}}^{-1}\mathbf{F}_{md}\mathbf{E}_d^T \tag{72}$$

$$\underset{\sim}{\mathbf{R}} = \mathbf{I} + \gamma \mathbf{F}_{md}\mathbf{F}_{md}^T \tag{73}$$

Calculations to determine $\mathbf{L}$ were done using the MATLAB routine *lqe.m* within the control toolbox.

Finally, the controller is put in the form of Eqs. (19–20) using the bilinear transformation (Antoniou, 1993) to yield the following compensator

$$\mathbf{x}_{k+1}^c = \underset{\sim}{\mathbf{A}}_c\mathbf{x}_k^c + \underset{\sim}{\mathbf{B}}_c\mathbf{y}_k^s \tag{74}$$

$$\mathbf{u}_k = \underset{\sim}{\mathbf{C}}_c\mathbf{x}_k^c + \underset{\sim}{\mathbf{D}}_c\mathbf{y}_k^s. \tag{75}$$

Calculations to determine the discrete time compensator were performed in MATLAB using the *c2dm.m* routine within the control toolbox. The SIMULINK block show in Fig. 10 is used to represent the sample control algorithm in the simulation.

Control System Performance

To assess the performance of the sample control strategy, a set of controlled simulations is performed for the pre- and post-earthquake evaluation models described previously. Note that the responses were determined through simulation using the SIMULINK program shown in Fig. 7. The contents of the SIMULINK blocks in Fig. 7 representing the sensors, control devices and control algorithm were replaced with those shown in Figs. 8–10. For the El Centro, Hachinohe, and Northridge earthquakes, the duration of the simulation was 100 seconds, and for the Kobe earthquake the duration was 180 seconds.

To calculate the evaluation criteria, all outputs of the structure were defined as evaluation outputs, thus $\mathbf{y}_e = [x_{\eta_1} \ldots x_{\eta_{20}}\ \dot{x}_{\eta_1} \ldots \dot{x}_{\eta_{20}}\ \ddot{x}_{a\eta_1} \ldots \ddot{x}_{a\eta_{20}}]^T$ (20 relative displacements, 20 relative

velocities, and 20 absolute accelerations). The maximum uncontrolled response values provided in Table 1 were used to calculate the evaluation criteria defined in Table 2.

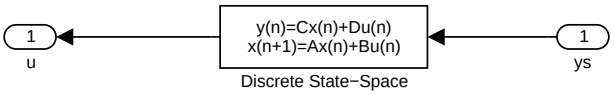

Figure 10: SIMULINK Block Representing the Control Algorithm for the Sample Control System Design.

The resulting evaluation criteria for this control design are presented in Table 3 (pre-earthquake) and Table 4 (post-earthquake). In these tables, the evaluation criteria are shown for each earthquake, and the maximum value over all four earthquakes is provided in the last column. Additionally, the maximum values of the control constraints are provided for each earthquake.

Although not intended to be a competitive design, note that for the pre-earthquake study, the first eight evaluation criteria are less than one, indicating that the controlled responses are lower than the uncontrolled responses. The control system reduces the maximum relative displacement by 15.9–35.7% and the maximum normalized drift by 11.9–33.7% as compared to the uncontrolled values. Figure 11 shows the responses of the roof of the structure over time for each earthquake. For clarity, only the first 80 seconds of the response is shown. In these plots one observes that the control system not only reduces the peak response, but is also able to relatively quickly dampen out the responses of the building. This observation is also supported by the significant reduction in the normed responses of the structure, indicated by the values of $J_5 - J_8$. Figure 11 also shows a series of plots portraying certain maximum responses of the structure. For each earthquake, the maximum value of the absolute acceleration at each above ground floor, and the maximum value of the non-dimensionalized interstory drift at each above ground floor, are plotted. Notice that for all earthquakes, a significant reduction in the non-dimensionalized maximum interstory drift is obtained in the controlled system. Additionally, the maximum absolute acceleration level is reduced from the uncontrolled value, although in most cases the acceleration is unaffected at the lower floors, there is a significant decrease in the peak acceleration levels at the upper floors.

Although the control law was designed based on the pre-earthquake model of the structure, the control strategy achieves significant response reduction in the post-earthquake structure as well. The maximum relative displacements and maximum non-dimensionalized interstory drifts of the structure are reduced by 5.3–32.1% and 4.8–24.7% of the uncontrolled values, respectively. Additionally, the structural responses are also substantially reduced, as demonstrated quantitatively by the values of the normed responses $J_5 - J_8$ and visually in Fig. 12 by the time histories of the displacement of the roof relative to the ground. Additionally, the plots in Fig. 12 portraying the maximum responses of the non-dimensionalized interstory drifts show that the maximum interstory drift is reduced substantially at every floor of the structure for every earthquake. The maximum absolute acceleration plots show that the acceleration levels at the upper floors are typically reduced significantly, although some increases in the acceleration levels are observed at the lower floors for the Hachinohe earthquake record.

Note that the sample control system meets all of the control constraints. As discussed previously, the control algorithm is based on feedback from five accelerometers with a sensitivity of 10V/*g*, and hydraulic actuators with a capacity of 897 kN (200 kips) are employed as the control devices. Furthermore, the requirements of the hydraulic actuators employed in this control system do not exceed the constraints of the devices (*i.e.*, maximum force capacity of 897 kN, maximum stroke of ±8.9 cm). The control algorithm has 62 states, which is deemed an acceptable number of states based on present day technology (dSpace 1997). Based on an eigenvalue analysis, the control algorithm is stable. Additionally, the maximum control signal over all of the four earthquakes is 6.32 V and 5.80 V, for the pre- and post-earthquake simulations, respectively, which is below the 10V limit. Finally, the performance of the control system, as demonstrated in the pre- and post-earthquake evaluation criteria, is indicative of the stability robustness of the closed loop system.

Closure

The models and data for the next generation benchmark control problem for seismically excited buildings is available in a set of MATLAB files. Included are scripts which build the pre- and post-earthquake evaluation models of the Los Angeles 20-story building, perform the sample control design and run the simulation. These files are available on the World Wide Web at the following URL:

http://www.nd.edu/~quake/

This information is also available on a mirror web site at:

http://www.seas.wustl.edu/research/quake/

If you cannot access the World Wide Web or have questions regarding the benchmark problem, please contact the senior author via e-mail at: spencer@nd.edu.

To increase the value of this effort to the community, participants in the benchmark study are requested to submit their control designs electronically for inclusion on the benchmark homepage cited previously. This electronic submission should be in the form of an m-file script and the associated data that, when run, produces the evaluation criteria used defined in the problem statement. The file *evalcrit.m* included with the sample control strategy is an example of the required evaluation m-file script. See the *README* file included with the downloaded benchmark data for more details.

Acknowledgments

The authors would like to thank SAC for making the plans available for the Los Angeles 20-story building. The support of the National Science Foundation under Grant No. CMS 95–28083 (Dr. S.C. Liu, program director) and the input provided by the many members of the structural control community are gratefully acknowledged.

Table 3: Pre-Earthquake Evaluation Criteria for the Sample Control Strategy.

	El Centro	Hachinohe	Northridge	Kobe	Max Value
J_1	0.83641	0.64297	0.84169	0.83707	0.84169
J_2	0.76526	0.66295	0.89064	0.77989	0.89064
J_3	0.90873	0.68122	0.73076	0.77925	0.90873
J_4	0.82445	0.68637	0.92953	0.75013	0.92953
J_5	0.67900	0.55644	0.56908	0.69826	0.69826
J_6	0.64982	0.53422	0.54936	0.73189	0.73189
J_7	0.56290	0.57347	0.59964	0.62149	0.62149
J_8	0.65736	0.53545	0.54906	0.70146	0.70146
J_9	$5.1430\text{x}10^{-3}$	$4.4520\text{x}10^{-3}$	$1.1703\text{x}10^{-2}$	$1.3881\text{x}10^{-2}$	$1.3881\text{x}10^{-2}$
J_{10}	$6.3221\text{x}10^{-2}$	$5.3661\text{x}10^{-2}$	$7.2224\text{x}10^{-2}$	$1.0050\text{x}10^{-1}$	$1.0050\text{x}10^{-1}$
J_{11}	$6.0031\text{x}10^{-3}$	$3.9088\text{x}10^{-3}$	$1.3172\text{x}10^{-2}$	$1.9699\text{x}10^{-2}$	$1.9699\text{x}10^{-2}$
J_{12}	$1.7602\text{x}10^{-2}$	$1.6059\text{x}10^{-2}$	$4.6692\text{x}10^{-2}$	$6.6554\text{x}10^{-2}$	$6.6554\text{x}10^{-2}$
J_{13}	50				
J_{14}	5				
J_{15}	62				
$\max_{i,t}\lvert u_i\rvert$ (V)	2.3322	2.0185	5.3437	6.3193	6.3193
$\max_{i,t}\lvert y_i^{\text{a}}\rvert$ (m)	$2.3998\text{x}10^{-2}$	$2.7745\text{x}10^{-2}$	$7.6493\text{x}10^{-2}$	$5.7171\text{x}10^{-2}$	$7.6493\text{x}10^{-2}$
$\max_{i,t}\lvert f^i\rvert$ (kN)	$2.7966\text{x}10^{2}$	$2.4208\text{x}10^{2}$	$6.3637\text{x}10^{2}$	$7.5479\text{x}10^{2}$	$7.5479\text{x}10^{2}$

Table 4: Post-Earthquake Evaluation Criteria for the Sample Control Strategy.

	El Centro	Hachinohe	Northridge	Kobe	Max Value
J_1	0.90540	0.95701	0.89536	0.67871	0.95701
J_2	0.78630	0.95220	0.87461	0.75342	0.95220
J_3	0.96364	0.98872	0.87791	0.86729	0.98872
J_4	1.0237	1.0098	1.0226	0.83770	1.0237
J_5	0.58421	0.58789	0.64182	0.49803	0.64182
J_6	0.61935	0.58410	0.62597	0.55642	0.62597
J_7	0.72267	0.63379	0.54427	0.61833	0.72267
J_8	0.58675	0.54101	0.57136	0.52146	0.58675
J_9	$4.7313\text{x}10^{-3}$	$4.0596\text{x}10^{-3}$	$1.0589\text{x}10^{-2}$	$1.2992\text{x}10^{-2}$	$1.2992\text{x}10^{-2}$
J_{10}	$7.5587\text{x}10^{-2}$	$9.5798\text{x}10^{-2}$	$9.7784\text{x}10^{-2}$	$8.9657\text{x}10^{-2}$	$9.7784\text{x}10^{-2}$
J_{11}	$4.3104\text{x}10^{-3}$	$2.8936\text{x}10^{-3}$	$1.2276\text{x}10^{-2}$	$1.4300\text{x}10^{-2}$	$1.4300\text{x}10^{-2}$
J_{12}	$1.6151\text{x}10^{-2}$	$1.3715\text{x}10^{-2}$	$4.3397\text{x}10^{-2}$	$4.9986\text{x}10^{-2}$	$4.9986\text{x}10^{-2}$
J_{13}	50				
J_{14}	5				
J_{15}	62				
$\max_{i,t}\lvert u_i\rvert$ (V)	2.0915	1.8060	4.7344	5.7984	5.7984
$\max_{i,t}\lvert y_i^{\text{a}}\rvert$ (m)	$2.1003\text{x}10^{-2}$	$2.8578\text{x}10^{-2}$	$8.8753\text{x}10^{-2}$	$5.8830\text{x}10^{-2}$	$8.8753\text{x}10^{-2}$
$\max_{i,t}\lvert f^i\rvert$ (kN)	$2.5728\text{x}10^{2}$	$2.2075\text{x}10^{2}$	$5.7581\text{x}10^{2}$	$7.0644\text{x}10^{2}$	$7.0644\text{x}10^{2}$

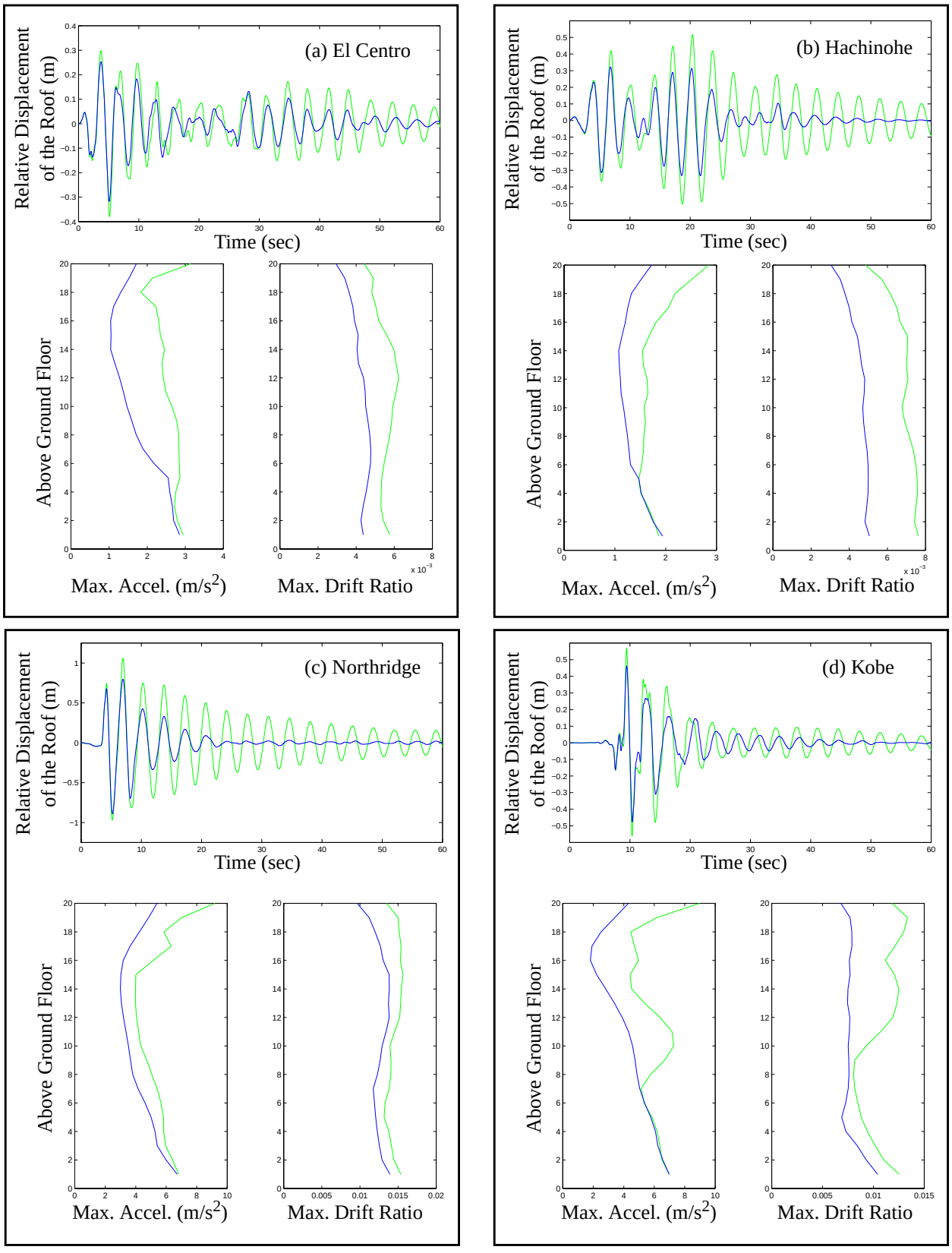

Figure 11: Uncontrolled (dotted) and Controlled (solid) Responses of the Pre-Earthquake Evaluation Model: a) El Centro b) Hachinohe c) Northridge d) Kobe.

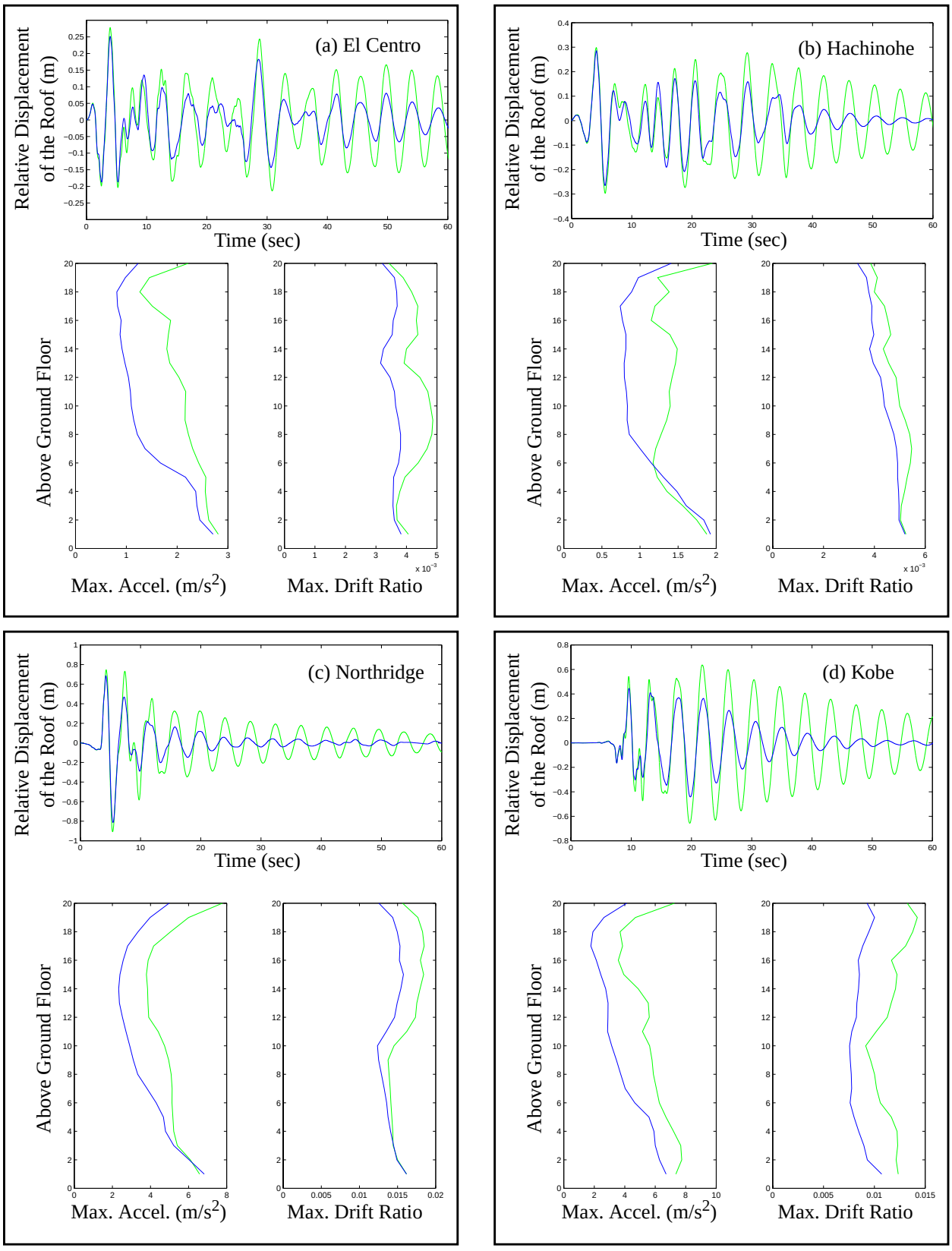

Figure 12: Uncontrolled (dotted) and Controlled (solid) Responses of the Post-Earthquake Evaluation Model: a) El Centro b) Hachinohe c) Northridge d) Kobe.

Appendix I – References

Antoniou, A. (1993). *Digital Filters: Analysis, Design, and Applications*, McGraw-Hill, Inc., New York, pp. 444–446.

Balas, G.J. (1997). "Synthesis of Controllers for the Active Mass Driver System in the Presence of Uncertainty." *Proceedings of the ASCE Structures Congress XV*, pp. 1270–1274.

Chen, J-C. Ed. (1996) *Proceedings of the 2nd International Workshop on Structural Control: Next Generation of Intelligent Structures*, Research Centre, The Hong Kong University of Science and Technology (see *http://cwis.usc.edu/dept/civil_eng/structural/welcome.html*).

Cook, R.D., Malkus, D.S., Plesha, M.E. (1989). *Concepts and Applications of Finite Element Analysis*, John Wiley & Sons, New York.

Craig, Jr., R.R. (1981). *Structural Dynamics, An Introduction to Computer Methods*, John Wiley & Sons, New York.

dSpace (1997). dSpace, Inc., Northville, Michigan.

Dyke, S.J., Spencer Jr., B.F., Quast, P. and Sain, M.K. (1995). "The Role of Control-Structure Interaction in Protective System Design." *Journal of Engineering Mechanics, ASCE*, Vol. 121, No. 2, pp. 322–338.

Fujino, Y., Soong, T.T. and Spencer Jr., B.F. (1996). "Structural Control: Basic Concepts and Applications." *Proceedings of the ASCE Structures Congress XIV*, Chicago, Illinois, pp. 1277–1287.

Housner, G.W., Masri, S.F., and Chassiakos, A.G., Eds. (1994). *Proceedings of the First World Conference on Structural Control*, International Association for Structural Control, Los Angeles.

Lu, J., and Skelton, R.E. (1997). "Covariance Control Using Closed Loop Modeling for Structures." *Proceedings of the ASCE Structures Congress XV*, pp. 1285–1289.

MATLAB (1997). The Math Works, Inc. Natick, Massachusetts.

Naeim, F. (1997). "Performance of Extensively Instrumented Buildings during the January 17, 1994 Northridge Earthquake," *JMA Report #97–7530.68*, Report on Contract #1093–557 to the Strong Motion Instrumentation Program, California Division of Mines and Geology, John A. Martin and Associates.

SIMULINK (1997). The Math Works, Inc. Natick, Massachusetts.

Sack, R.L. (1989). *Matrix Structural Analysis*, PWS-Kent Pub. Co., Boston.

Skelton, R.E. (1988). *Dynamic Systems Control: Linear Systems Analysis and Synthesis*. Wiley, New York.

Smith, H.A., Breneman, S.E. and Sureau, O. (1997). "H–infinity Static and Dynamic Output Feedback Control of the AMD Benchmark Problem." *Proceedings of the ASCE Structures Congress XV*, pp. 1280–1284.

Soong, T.T. (1990). *Active Structural Control: Theory and Practice*, Longman Scientific and Technical, Essex, England.

Soong, T.T. and Grigoriu, M. (1993). *Random Vibration of Mechanical and Structural Systems*, Prentice–Hall, Englewood Cliffs, New Jersey.

Soong, T.T. and Constantinou, M.C., Eds. (1994). *Passive and Active Structural Vibration Control in Civil Engineering*, CISM Lecture Notes, Springer–Verlag, New York.

Spencer Jr., B.F., Dyke, S.J. and Deoskar, H.S. (1997). "Benchmark Problems in Structural Control – Part I: Active Mass Driver System." *Proceedings of the ASCE Structures Congress XV*, Vol. 2, pp. 1265–1269.

Spencer Jr., B.F. and Sain, M.K. (1997) "Controlling Buildings: A New Frontier in Feedback," *IEEE Control Systems Magazine: Special Issue on Emerging Technologies* (Tariq Samad Guest Ed.), Vol. 17, No. 6, pp. 19–35.

Spencer Jr., B.F., Dyke, S.J. and Deoskar, H.S. (1998). "Benchmark Problems in Structural Control – Part I: Active Mass Driver System and Part II: Active Tendon System." *Earthquake Engineering and Structural Dynamics*, to appear.

Stengel, R.F. (1986). *Stochastic Optimal Control: Theory and Application*. Wiley, New York.

Wu, J.C., Agrawal, A.K. and Yang J.N. (1997). "Application of Sliding Mode Control to a Benchmark Problem." *Proceedings of the ASCE Structures Congress XV*, pp. 1275–1279.

Yang, J.N., Wu, J.C., Samali, B. and Agrawal, A.K. (1998). "A Benchmark Problem For Response Control of Wind-Excited Tall Buildings." *Proceedings of the 2nd World Conference on Structural Control* (also see *http://www.eng.uci.edu/~anil/benchmark.html*).

Appendix II – Nomenclature

$\mathbf{A}$ – cross-sectional area of the actuator

$\tilde{\mathbf{A}}$ – matrix used in the solution of the algebraic Riccati equation

$\underset{\sim}{\mathbf{A}}$ – matrix used in the solution of the algebraic Riccati equation

$\mathbf{A}, \mathbf{B}, \mathbf{E}$ – state space matrices for the evaluation model

$\mathbf{A}_a, \mathbf{B}_a, \mathbf{C}_a, \mathbf{D}_a$ – state space matrices for the hydraulic actuator model

$\underset{\sim}{\mathbf{A}}_c, \underset{\sim}{\mathbf{B}}_c, \underset{\sim}{\mathbf{C}}_c, \underset{\sim}{\mathbf{D}}_c$ – state space matrices for the feedback compensator

$\mathbf{A}_d, \mathbf{B}_d, \mathbf{E}_d$ – state space matrices for the design model

$\mathbf{A}_r, \mathbf{B}_r, \mathbf{E}_r$ – state space matrices for the reduced order evaluation model

$\mathbf{A}_s, \mathbf{B}_s, \mathbf{C}_s, \mathbf{D}_s, \mathbf{E}_s, \mathbf{F}_s$ – state space matrices for the sensor model

a_1, a_2, a_3 – hydraulic actuator model parameters

β – bulk modulus of the hydraulic fluid

$\tilde{\mathbf{C}}$ – evaluation model damping matrix

$\mathbf{C}_c, \mathbf{D}_c, \mathbf{F}_c$ – state space matrices for the evaluation model used to specify the outputs used in the control device dynamics model(s)

$\mathbf{C}_{cr}, \mathbf{D}_{cr}, \mathbf{F}_{cr}$ – state space matrices for the reduced order evaluation model used to specify the connection responses

$\mathbf{C}_e, \mathbf{D}_e, \mathbf{F}_e$ – state space matrices for the evaluation model used to specify the outputs for system evaluation

$\mathbf{C}_m, \mathbf{D}_m, \mathbf{F}_m$ – state space matrices for the evaluation model used to specify the measured outputs

$\mathbf{C}_{md}, \mathbf{D}_{md}, \mathbf{F}_{md}$ – state space matrices for the design model used to specify measured responses

$\mathbf{C}_{mr}$, $\mathbf{D}_{mr}$, $\mathbf{F}_{mr}$ – state space matrices for the reduced order evaluation model used to specify the measured responses

$\mathbf{C}_{wd}$, $\mathbf{D}_{wd}$, $\mathbf{F}_{wd}$ – state space matrices for the design model used to specify regulated responses

$\mathbf{C}_{wr}$, $\mathbf{D}_{wr}$, $\mathbf{F}_{wr}$ – state space matrices for the reduced order evaluation model used to specify the regulated responses

d_i – interstory drift of above ground floors (m)

d_n^{max} – maximum interstory drift ratio for each respective earthquake

$\left\| d_n^{max} \right\|$ – the maximum normed interstory drift ratio corresponding to the uncontrolled structure excited by each respective earthquake $(\sqrt{\text{sec}})$

E – parameter used in the infinite horizon performance index for the sample LQG

F_b^{max} – maximum base shear (kN)

$\left\| F_b^{max} \right\|$ – the maximum normed uncontrolled base shear for each respective earthquake $(\text{kN} \cdot \sqrt{\text{sec}})$

$\mathbf{f}$ – vector of forces produced by the control device(s) (kN)

$\mathbf{f}_m$ – the continuous time vector of measured responses of the control device(s)

f^i – control force of the *i*th control device (kN)

$\hat{\mathbf{G}}$ – vector defining the loading of ground acceleration onto the evaluation model after boundary conditions are applied

$\tilde{\mathbf{G}}$ – vector defining the loading of ground acceleration onto the evaluation model after the Guyan reduction

$\underset{\sim}{\mathbf{G}}$ – matrix used in the solution of the algebraic Riccati equation

g – gravitational constant (9.81 m/sec^2)

$\mathbf{g}_1(\cdot)$, $\mathbf{g}_2(\cdot)$ – sensor dynamics for the sensor(s)

$\mathbf{g}_3(\cdot)$, $\mathbf{g}_4(\cdot)$ – functions defining the feedback compensator(s)

$\mathbf{g}_5(\cdot)$, $\mathbf{g}_6(\cdot)$, $\mathbf{g}_7(\cdot)$, $\mathbf{g}_8(\cdot)$ – dynamics functions for the control device(s)

h_i – height of each of the stories: $h_1 = 5.49$ m; $h_i = 3.96$ m, $i = 2, \ldots, 20$

$\underset{\sim}{\mathbf{H}}$ – matrix used in the solution of the algebraic Riccati equation

$\mathbf{I}$ – identity matrix

J_i – *i*th evaluation criteria

$\hat{J}$ – infinite horizon performance index

$\mathbf{K}$ – global stiffness matrix of structure after boundary conditions are applied

$\hat{\mathbf{K}}$ – global stiffness matrix after the constraints are applied

$\tilde{\mathbf{K}}$ – global stiffness matrix after the Guyan reduction

$\underset{\sim}{\mathbf{K}}$ – full state feedback gain matrix for the deterministic regulator problem

$\mathbf{K}_{aa}$, $\mathbf{K}_{ad}$, $\mathbf{K}_{da}$, $\mathbf{K}_{dd}$ – partitioned global stiffness matrix of structure after boundary conditions are applied in terms of active (a) and dependent (d) DOFs

$\hat{\mathbf{K}}_{aa}$, $\hat{\mathbf{K}}_{ad}$, $\hat{\mathbf{K}}_{da}$, $\hat{\mathbf{K}}_{dd}$ – partitioned global stiffness matrix of structure after the constraints are applied in terms of active (a) and dependent (d) DOFs

k – discrete time step index

k_q, k_c – actuator model system constants

$\mathbf{L}$ – Kalman Filter optimal estimator

$\mathbf{M}$ – global mass matrix of structure after boundary conditions are applied

$\hat{\mathbf{M}}$ – global mass matrix after the constraints are applied

$\tilde{\mathbf{M}}$ – global mass matrix after the Guyan reduction

$\mathbf{M}_{aa}$, $\mathbf{M}_{ad}$, $\mathbf{M}_{da}$, $\mathbf{M}_{dd}$ – partitioned global mass matrix of structure after boundary conditions are applied in terms of active (a) and dependent (d) DOFs

$\hat{\mathbf{M}}_{aa}$, $\hat{\mathbf{M}}_{ad}$, $\hat{\mathbf{M}}_{da}$, $\hat{\mathbf{M}}_{dd}$ – partitioned global mass matrix of structure after the constraints are applied in terms of active (a) and dependent (d) DOFs

m_i – seismic mass (including framing) of the above-ground floor: $m_1 = 2.83\times10^5$ kg; $m_i = 2.76\times10^5$ kg, $i = 2, \ldots, 19$; $m_{20} = 2.92\times10^5$ kg

$\tilde{\mathbf{N}}$ – matrix used in the solution of the algebraic Riccati equation

n – global DOF

$\mathbf{P}$ – vector defining the loading of control forces onto the structure after boundary conditions are applied

$\hat{\mathbf{P}}$ – vector defining the loading of control forces onto the model after the constraints are applied

$\tilde{\mathbf{P}}$ – vector defining the loading of control forces onto the model after Guyan reduction

$\underset{\sim}{\mathbf{P}}$ – solution of the algebraic Riccati equation

$\mathcal{P}_i$ – measure of the instantaneous power required by the active control actuators

$\|\mathcal{P}_i\|$ – measure of the total power required by the ith actuator for the entire seismic event

$\mathbf{Q}$ – weighting matrix for LQG control design

$\tilde{\mathbf{Q}}$ – matrix used in the solution of the algebraic Riccati equation

$\mathbf{R}$ – diagonal matrix used in the LQG control design

$\tilde{\mathbf{R}}$ – matrix used in the solution of the algebraic Riccati equation

$\underset{\sim}{\mathbf{R}}$ – matrix used in the solution of the algebraic Riccati equation

$\mathbf{R}_{\mathrm{da}}, \mathbf{R}_{\mathrm{dd}}$ – matrices relating the active and dependent DOF of floors

$\mathbf{S}$ – solution of the algebraic Riccati equation

$S_{v_i v_i}$ – autospectral density function of measurement noise

$S_{\ddot{x}_g \ddot{x}_g}$ – autospectral density function of ground acceleration

T – sampling time (sec)

$\mathbf{T}_{\mathrm{da}}$ – transformation sub-matrix for Ritz transformation

$\hat{\mathbf{T}}_{\mathrm{da}}$ – transformation sub-matrix for Guyan reduction

$\mathbf{T}_{\mathrm{G}}$ – transformation matrix for Guyan reduction

$\mathbf{T}_{\mathrm{R}}$ – transformation matrix for Ritz transformation

t – continuous time step index (sec)

t_{f} – sufficiently large time to allow the response of the structure to attenuate (sec)

$\mathbf{U}$ – response vector

$\mathbf{U}_{\mathrm{a}}$ – active DOFs of the response vector for the Ritz transformation

$\mathbf{U}_{\mathrm{d}}$ – dependent DOFs of the response vector for the Ritz transformation

$\tilde{\mathbf{U}}$ – vector of DOFs ordered for the Guyan reduction

$\mathbf{u}$ – continuous vector control output (sample and hold of $\mathbf{u}_k$) (Volts)

$\mathbf{u}_k$ – vector control output at time $t = kT$ for the feedback compensator (Volts)

V – characteristic hydraulic fluid volume for the actuator

$\mathbf{v}$ – measurement noise vector for the evaluation model

W – seismic weight of one N-S MRF (54,377 kN)

$\mathbf{x}$ – state vector for the evaluation model

x_i – ith state of evaluation model

$\mathbf{x}_k^{\mathrm{c}}$ – state vector for the discrete feedback compensator at time $t = kT$

$\mathbf{x}^{\mathrm{a}}$ – continuous state vector for the control device model

$x^{\max}$ – maximum uncontrolled displacement relative to ground for each respective earthquake (m)

$\left\| x^{\max} \right\|$ – the maximum normed uncontrolled displacement for each respective earthquake $(\mathrm{m} \cdot \sqrt{\mathrm{sec}})$

$\mathbf{x}^{\mathrm{d}}$ – continuous state vector for the design model

$\hat{\mathbf{x}}^{\mathrm{d}}$ – Kalman Filter estimate of the state vector for the design model

$\mathbf{x}^{\mathrm{r}}$ – state vector of the reduced order model of the structure

$\mathbf{x}^{\mathrm{s}}$ – state vector of the sensor model

$\dot{x}^{\max}$ – maximum uncontrolled velocity relative to ground (m/sec)

$\ddot{x}_{\mathrm{a}i}$ – absolute acceleration of the *i*th state ($\mathrm{m/sec}^2$)

$\ddot{x}_{\mathrm{a}}^{\max}$ – maximum uncontrolled absolute roof acceleration ($\mathrm{m/sec}^2$)

$\left\| \ddot{x}_{\mathrm{a}}^{\max} \right\|$ – the maximum normed absolute acceleration of the uncontrolled structure excited by each respective earthquake $(\mathrm{m} \cdot \mathrm{sec}^{-3/2})$

$\ddot{x}_{\mathrm{g}}$ – absolute acceleration of the ground ($\mathrm{m/sec}^2$)

y_i^{a} – displacement of the *i*th control device (m)

$\dot{y}_i^{\mathrm{a}}$ – velocity of the *i*th control device (m/sec)

$\mathbf{y}_{\mathrm{c}}$ – vector of responses of evaluation model for actuator model determination

$\mathbf{y}_{\mathrm{cr}}$ – vector of connection responses of reduced order evaluation model

$\mathbf{y}_{\mathrm{e}}$ – vector of responses of evaluation model for control strategy evaluation

$\mathbf{y}_{\mathrm{f}}$ – the vector of control device responses used for evaluation purposes

$\mathbf{y}_{\mathrm{m}}$ – vector of measured responses of evaluation model

$\mathbf{y}_{\mathrm{md}}$ – vector of measured responses of design model

$\mathbf{y}_{\mathrm{mr}}$ – vector of measured responses of reduced order evaluation model

$\mathbf{y}^{\mathrm{s}}$ – vector of responses of sensor model

$\mathbf{y}_k^{\mathrm{s}}$ – discrete vector of responses of sensor model

$\mathbf{y}_{\mathrm{wd}}$ – vector of regulated responses of design model

$\mathbf{y}_{\mathrm{wr}}$ – vector of regulated responses of reduced order evaluation model

γ – proportional feedback gain stabilizing the actuator

$\mathbf{\Gamma}$ – vector defining the loading of ground acceleration onto the unreduced model

$\mathbf{\Delta}$ – matrix to transform floor displacements to control device displacements

$\boldsymbol{\eta}$ – the set of states corresponding to the horizontal displacement of above ground floors (level 2–roof) relative to the ground

$\boldsymbol{\theta}$ – vector of actuator model parameters used in design model coefficient matrices

$\boldsymbol{\Phi}$ – matrix of eigenvectors of $\tilde{\mathbf{M}}^{-1}\tilde{\mathbf{K}}$

ζ_i – damping in the ith mode of the evaluation model

ω_i – natural (undamped) frequency of the ith mode of the evaluation model

$|\cdot|$ – absolute value operator

$\|f(t)\| \equiv \sqrt{\int_0^{t_f} f^2(t)dt}$ – L_2-norm of the function $f(t)$ on the time interval $[0, t_f]$